Escola de Camins
Escola Tècnica Superior d'Enginyeria de Camins, Canals i Ports
UPC BARCELONATECH

# MASTER THESIS

**Master**

Numerical Methods in Engineering

**Title**

Validation of a non-linear shell code

**Author**

Pedro Bonilla Villalba

**Tutor**

Riccardo Rossi,
Massimo Petracca

**Intensification**

**Date**

14th of July of 2014

UPC RMEE

# Validation of a non-linear shell code

Mechanics of Materials and Structures Department
Universitat Politècnica de Catalunya, UPC BARCELONATECH

Pedro Bonilla Villalba
Master Thesis

# ABSTRACT

This work presents a series of benchmarks and the consequent analysis of the results for the non-linear shell element implementation within Kratos program of CIMNE research organization at the UPC BARCELONATECH University.

The theoretical basis of the shell elements is the corotational (CR) formulation of finite elements.

The benchmarks were selected to demonstrate the efficiency and accuracy of the present shell elements under several linear and non-linear stress/strain cases with small and large displacements. All the results of the shell elements showed good agreement with the references or the analytical solution.

Comparison with other commercial codes (Abaqus and Xfinas) was also made in order to establish not only the correctness of the formulation but the accuracy towards current standards.

**Key words:** benchmarks, validation, nonlinear structural analysis, corotational description, shell finite elements, Kratos.

# INDEX

# 1. INTRODUCTION

The objective of this work is to validate the shell type elements within Kratos program. The theoretical basis of the shell elements is the co-rotational (CR) formulation of finite elements by Carlos A. Felippa and Bjorn Haugen, and the implementation of the code into the program was done by Massimo Petracca, external tutor of this master thesis.

Validation is a needed process to check the correctness of the theory behind the finite element, but also the implementation of the program. This process has the double purpose of being a quality control of the software previous to the release to the user and to detect situations in which the mathematical model of the element is not efficient enough allowing us to focus the research of future improvements.

The elements that have been tested are quadrilateral thick elements with 4 nodes and triangular thin elements with 3 nodes and uniformly reduced integration to avoid shear and membrane locking, which are the elements implemented at the moment when this master thesis was written.

In order to validate the fore-mentioned shell elements, the patch test, distortion test and other various numerical tests are carried out using GiD and Kratos. Kratos is a framework for building multi-disciplinary finite element programs and GiD is a pre and post-processor for numerical simulations in science and engineering. Both programs are developed by CIMNE research organization at the UPC BARCELONATECH University.

The different benchmarks tested were selected to demonstrate the efficiency and accuracy of the present shell elements towards different strain/stress states. The linear benchmarks tested in this thesis are normalized and compared with the analytical solution. For the non-linear benchmarks, NAFEMS tests have been used, since they have become the standard method of improving and verifying the accuracy of codes. The exception is the non-linear post-buckling analysis benchmark whose reference publication is G. Dhatt. 1970 [24].

All the results of the shell elements showed very good agreement with the references or the analytical solution, furthermore, comparison of the obtained results with known published program validation documentation such as Abaqus or Xfinas, confirm the similar or best performance than other classical formulations implemented in those commercial programs.

# 2. COROTATIONAL FORMULATION THEORY

## *2.1. COROTATIONAL FORMULATION MAIN CONCEPTS*

Before exploring the benchmarks, this chapter will introduce the basic aspects of the formulation of the shell elements. For deeper documentation on the topic the reference paper is C. A. Felippa and B. Haugen C, 2005 [1]. The publication states a unified formulation from the most relevant publications about the issue.

The key assumptions behind unified theoretical framework for the corotational formulation are:

(i) strains from a corotated configuration are small while

(ii) the magnitude of rotations from a base configuration is not restricted

The element internal force and consistent tangent stiffness matrix are derived by taking variations of the internal energy with respect to nodal freedoms.

The Corotational (CR) description is the most recent of the three in present use Lagrangian kinematic descriptions for finite element analysis of geometrically non-linear structures, and it is also the least developed one. The other 2 descriptions are Total Lagrangian (TL) and Updated Lagrangian (UL).

Since the three descriptions are Lagrangian kinematics, all of them follow the body (shell element for the purpose of this work) as it moves. The main difference between the CR formulation and the other two is that its domain of application is limited by a priori kinematic assumption:

**Displacements and rotations may be arbitrarily large, but deformations must be small.**

The CR formulation introduces the splitting of the Lagrangian tracking of the deformed body into two additive components. The first component tracks the rigid body motion part (including rotation) and the other one tracks just the deformation from the displaced and rotated original shape.

The following figure shows schematically the decomposition of the Lagrangian mapping from the original configuration $C^0$to the current or spatial configuration, which is called $C^D$for deformed, with an intermediate step called$C^R$or corotated, which only has into account the solid rigid motion.

*Figure 1*

*CR kinematic description.*

*$C^0$ is the initial, original, undeformed or material configuration.*

*$C^R$ is the corotated configuration considering only rigid body motion. The associated coordinate system is Cartesian and follows the element like a ghost or shadow.*

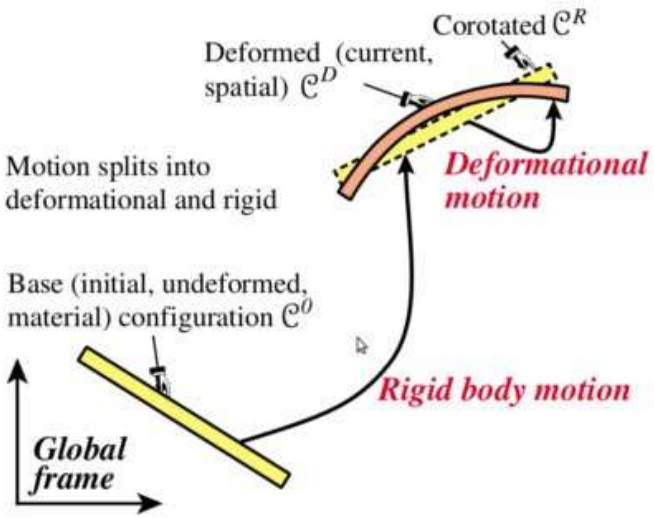


*$C^D$ Is the deformed, current or spatial configuration and considers only deformational motion respect $C^R$.*

## *2.2. COROTATIONAL FORMULATION APPLIED TO FEM*

The co-rotational concept in the continuum mechanics field has been known from 2 centuries ago. It has been applied since the beginning of the XX century to the study of whole structures, and Fraeijs de Veubeke 1976 [2] made a systematic formulation of the previous approaches closing the subject for whole structures. The “shadowing problem” approach presents the drawback of the non-uniqueness orienting a corotated Cartesian frame in case of axis symmetry of the body, which is frequent in aeronautics, being the main field of use.

It has not been since the last decades of XX century that has been used as part of FEM improvement research. Crisfield 1990, 1997, 1997 [3–5], developed the concept of “consistent CR formulation” where the stiffness matrix appears as the true variation of the internal force. Rankin [6] and Brogan at Lockheed introduced the concept of “element independent CR formulation” or EICR, which was improved in a series of publications by Rankin, Nour-Omid and coworkers [7–12]. While the EICR formulation benefits conceptually from the shadowing problem it uses projection operators to avoid the use of explicit “shadow” configurations.

The frame for nonlinear thin shell analysis introduced by Haugen 1994 [13], combines tools from the EICR (projectors and spins) with the shadow element concept and assumed strain element formulation. It is able to generate a set of hierarchical CR formulations and the use of spins instead of rotations for incremental nodal freedoms simplifies the EICR "front end" and facilitates attaining consistency.

Kratos program uses this formulation applied to geometrically nonlinear structural analysis shell elements. The main modifications from the Fraeijs de Veubeke's idea are:

1. Multiple Frames. One CR frame per finite element is introduced, instead of one CR frame for the whole structure.

2. Geometric-Based RBM Separation. The rigid body motion is separated directly from the total element motion using elementary geometric methods. For instance in a 2-node bar or beam one axis is defined by the displaced nodes, while for a 3-node triangle two axes are defined by the plane passing through the points, as shown in next figure.

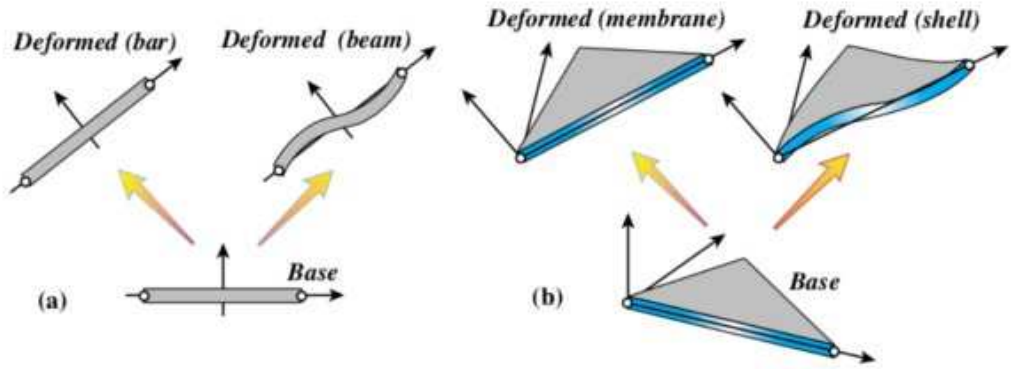


*Figure 2: Geometric-Based RBM Separation in the tracking of CR discrete elements (a) beams, (b) membrane/shells*

Taking as summary a paragraph of the Haugen's publication:

“In the co-rotation approach, the deformational part of the displacement is extracted by purging the rigid body components before any element computation is performed. This pre-processing of the displacements may be performed outside the standard element routines and thus is independent of element type (except for slight distinctions between beams, triangular and quadrilateral elements).”

The following figure summarize the way EICR splits the rigid body motion part and the deformational part of the problem into the code. The flow chart is mainly conceptual. For computational efficiency the interface logic may be embedded with each element through in lining techniques.

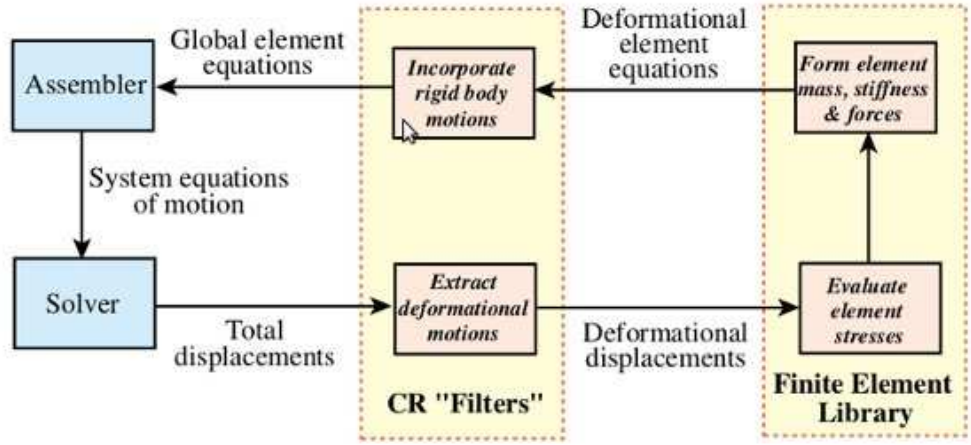


*Figure 3: Flow chart for CR “Filters” and FEM Library, solver and Assembler.*

# 3. SHELL ELEMENTS IMPLEMENTED IN KRATOS

Currently, the implementation in of the shell elements is under development in the Kratos program, as stated in the introduction.

The two elements that are already implemented and which this work tests are the triangular thin element with 3 nodes, and the quadrilateral thick element with 4 nodes and reduced integration.

As expanded below, CR formulation is the Element-Independent CR formulation, so it is common for both elements, but the computation of the Internal Forces and the Tangent (material) Stiffness matrix depends on the thickness of the element (considering or not transverse shear locking) and on the shape of the element (triangular and quadrilateral elements have different ways to confront membrane shear locking).

The scheme of implementation is:

At any given time step, and iteration the following steps are followed:

The 'Corotational Filter' removes the rigid body displacements/rotations:

[(Total_Displacements_Rotations - Rigid_Displacements_Rotations =

= Deformational(Small)_Displacement_Rotations]

Once removed, everything is transformed from global to local coordinate system, which consists in a set of coordinates for each shell element.

Within the local coordinates, the computation of the Internal Forces (-Fi) and the Tangent (material) Stiffness matrix (Km) of one of the 'Core Elements (for small displacements)' is performed. In this step lays the main difference among the two elements can be found.

a) Quadrilateral Thick Element:

For thick plates transverse shear locking arises, and consequently Reissner-Midlin Thick MITC4 shell formulation is implemented.

Regarding the membrane shear locking phenomenon, the formulation implemented is EAS (Enhanced Assumed Strains) stated by C. J. Simo and M. S. Rifai 2003 [14].

b) Triangular Thin Element:

DKT Discrete Kirchhoff Triangle shell formulation is implemented.

Regarding the membrane shear locking phenomenon, the formulation implemented is ANDES (Assumed Natural Deviatoric Strains) stated by C. A. Felippa 2003 [15]

In the next step the 'Corotational Filter' re-applies rigid body displacements and rotations to the deformational ones just computed.

Then the contribution of geometric nonlinearity is added.

$$Ke = Km + Kg \text{ (Geometric stiffness matrix)}$$

Finally, transformation back from local to global coordinate system is applied.

.

# 4. LINEAR STATIC ANALYSIS OF ISOTROPIC SHELL ELEMENT

## *4.1. TAPERED AND SWEPT BEAM*

The tapered and swept beam is a plane stress problem consisting in a trapezoidal beam subjected to a linear load on the free edge. The loading leads the free edge to rotate over the upper part of the clamping were the compression stress is concentrated in both directions, and all the lower and free edge part of the beam is subjected to tensile stress.

This simple 2D problem has analytical solution stated in Simo et al. 1989 [16] so it was the first element to test. In order to compare the numerical solution obtained with other elements, the 4 and 3 point nodes from the software Xfinas was the reference.

### Problem description

The trapezoidal 2D beam is clamped by a vertical edge of 44 unit length. The opposite free edge of 16 units length is also vertical, the length between them is 28 units and the lower point of the free edge is horizontal coincident with the upper point of the clamped edge. The 2 remaining edges complete the trapezoid.

Since Kratos shell GiD interface has not implemented the plane stress type of problem, apart from the clamping, Uz=0, Rx=0 and Ry=0 Boundary Conditions were stated.

The shell has 1 unit thickness and as material properties, Poisson's ratio 0.33 and Young's Modulus 1 in any consistent unit system.

All over the free edge a uniform vertical distributed load of total value 1.0 is applied.

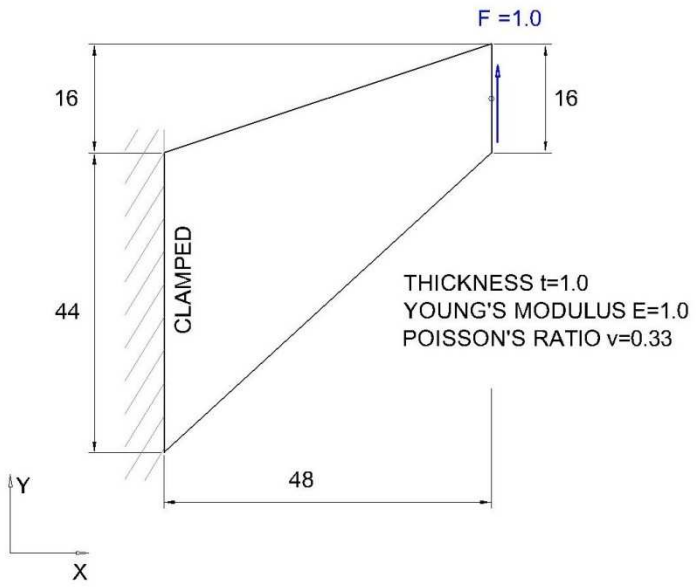


*Figure 1*

*Problem geometry and material properties*

Three different types of meshes are used in the test, with several refinements. The regular quadrilateral 2x2 mesh is the coarser mesh, and is refined by doubling the elements per edge at each refinement leading to 4x4, 8x8, 16x16 and 32x32 meshes.

The other 2 meshes consist in just splitting the quadrilateral meshes by the diagonals, being the mesh1 from bottom left corner to upper right and mesh 2 the other diagonal. Using different triangular meshes allow us to check the impact of mesh orientation and a bit of skew sensitivity for both elements.

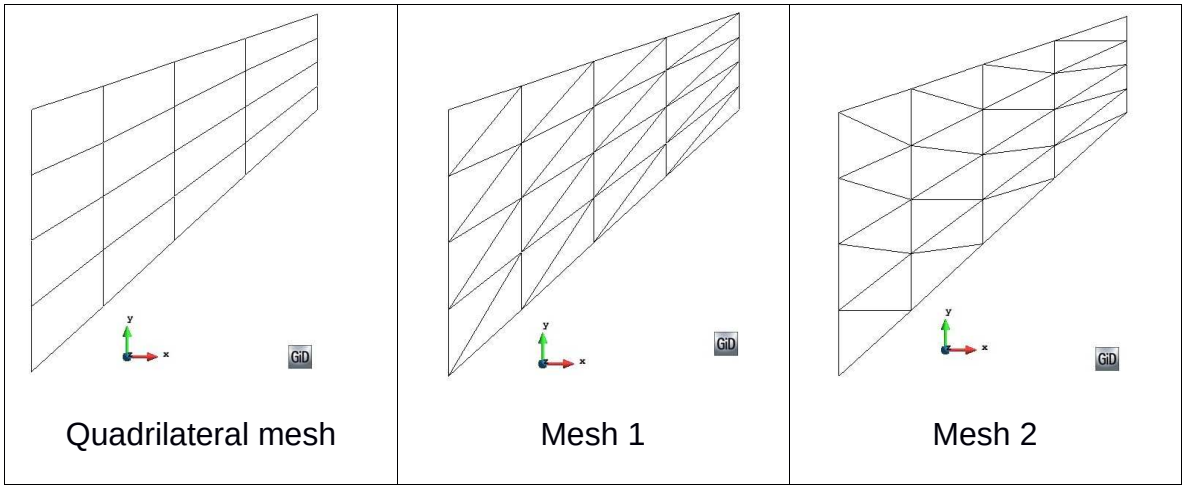


*Figure 2. Meshes used for tapered and swept beam*

## Results

As advanced in the problem description, the deformation consist on the lifting (in xy plane) of the free edge that turns into a general rotation over the upper part of the clamped edge due to the internal forces.

Consequently with the deformation, upper left part of the beam is compressed and lower right part tensioned, while shear follows the load direction.

Attached next are the figures showing the final deformed state, and the compression and tension stresses for some random meshes.

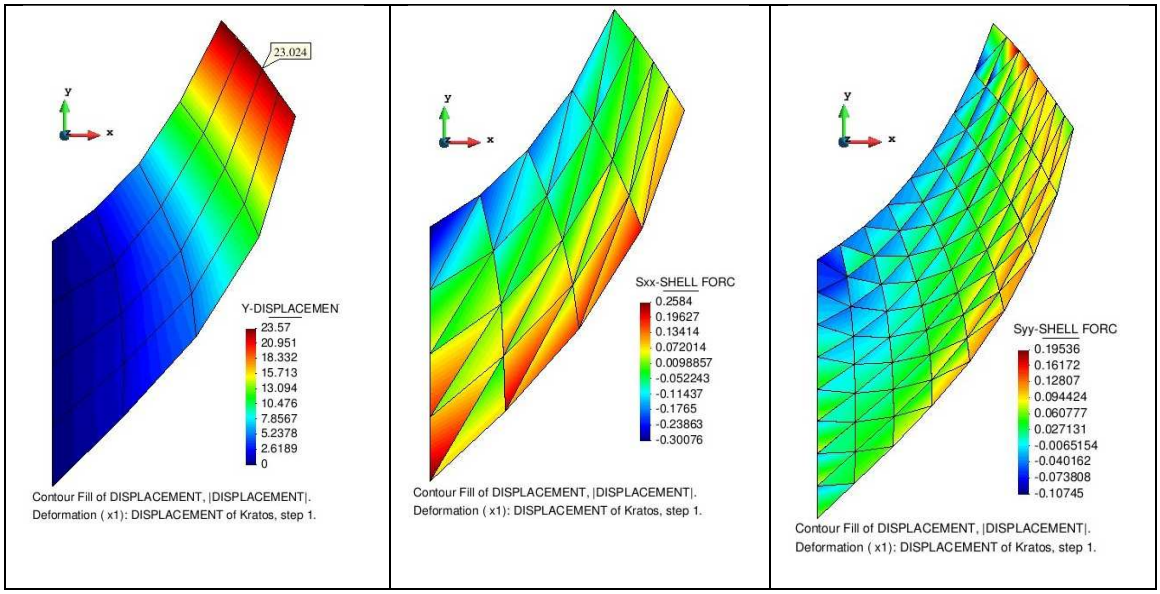


*Figure 3 displacements, Sx and Sy shell forces for different meshes.*

The magnitude of interest for comparison with analytical solution and xshell41 and xshell31 Xfinas elements is the y tip displacement (the center pint of the free edge).

| | | **TIP Y DISPLACEMENT** | | **RELATIVE ERROR** | |
|---|---|---|---|---|---|
| Analytical solution | | | 23.91 | | |
| | mesh | Xshell41 | Triangular thin Kratos | **Xshell41** | **Triangular thin Kratos** |
| Quadrilateral | 2x2 | 16.594 | 22.0090 | **-30.60%** | **-7.95%** |
| | 4x4 | 19.511 | 23.0240 | **-18.40%** | **-3.71%** |
| | 8x8 | 22.404 | 23.6540 | **-6.30%** | **-1.07%** |
| | 16x16 | 23.480 | 23.8620 | **-1.80%** | **-0.20%** |
| | 32x32 | 23.814 | 23.9260 | **-0.40%** | **0.07%** |
| | | Xshell31 | Triangular thin Kratos | **Xshell31** | **Triangular thin Kratos** |
| Triangular Mesh 1 | 2x2 | 16.689 | 17.9120 | **-30.20%** | **-25.09%** |
| | 4x4 | 21.280 | 20.5370 | **-11.00%** | **-14.11%** |
| | 8x8 | 23.145 | 22.4000 | **-3.20%** | **-6.32%** |
| | 16x16 | 23.719 | 23.3660 | **-0.80%** | **-2.28%** |
| | 32x32 | | 23.7290 | | **-0.76%** |
| Triangular Mesh 2 | 2x2 | 19.248 | 18.5160 | **-19.50%** | **-22.56%** |
| | 4x4 | 21.495 | 21.6520 | **-10.10%** | **-9.44%** |
| | 8x8 | 23.432 | 23.1110 | **-2.00%** | **-3.34%** |
| | 16x16 | 23.814 | 23.6670 | **-0.40%** | **-1.02%** |
| | 32x32 | | 23.8540 | | **-0.23%** |

The next plots show the evolution of the relative error versus the number of elements in one side.

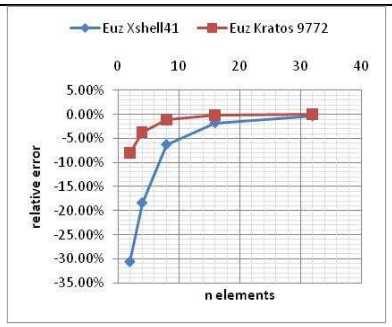


Quadrilateral mesh

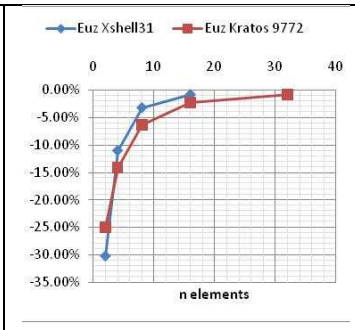


Triangular Mesh 1

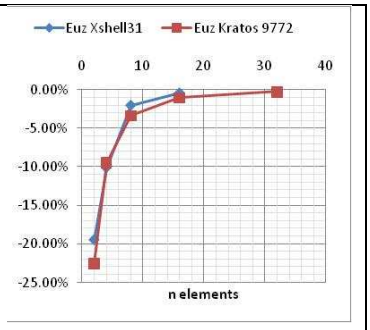


Triangular Mesh 2

*Figure 4, Relative error versus n of elements in one side*

It can be seen that the numerical solution is converging towards the reference one even though for the last quadrilateral fine mesh, the relative error changes of sign. Comparing the numerical results leads to the conclusion that both Kratos elements achieved the expected accuracy. Furthermore, comparing the results with Xfinas elements, it can be seen that triangular element had equivalent performance, while quadrilateral element showed better performance, since for all the quadrilateral meshes, Kratos result has less than half relative error than Xfinas element.

Regarding convergence, the three meshes present an almost constant slope. This behavior is good since allows to improve linearly the accuracy by refining the mesh.

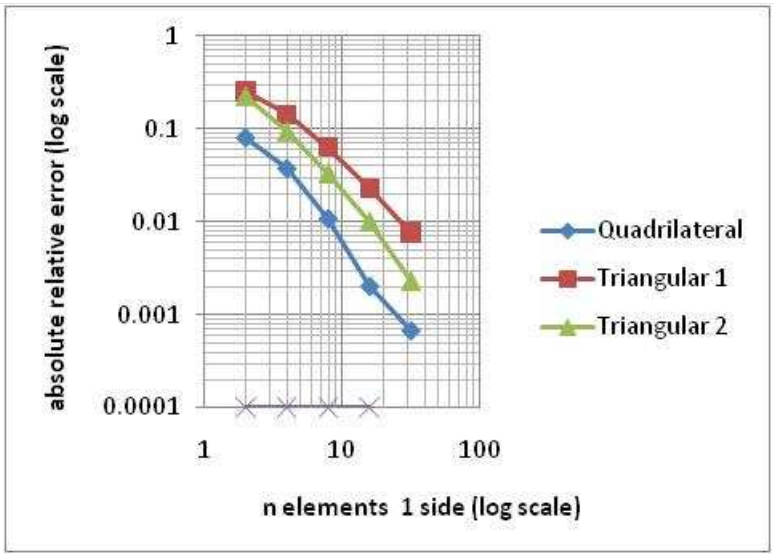


*Figure 5 convergence analysis (abs of relative error vs. n elements log scale) for the elements in the 3 meshes used.*

## *4.2. PURE BENDING OF A CANTILEVER BEAM SUBJECT TO END MOMENT*

It is usual to perform this test as an initial problem tackle in order to test the accuracy of the element under extreme inextensional bending and large deformation. This problem consisting in a straight cantilever subjected to a concentrated free end moment, has been analyzed by a number of researches, and has analytical solution. To further information see Bathe and Bolourchi 1979 [17].

For the proposed problem, the only non-trivial deformation component is the flexural one on the YZ plane (XY in the GiD implemented model). Moreover, according to the classical Euler formula, this bending deformation is constant along the beam, and it follows the curve described in the figure on the right.

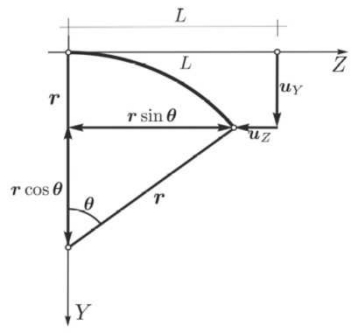


Although this is a linear test, the test was performed with a quasistatic strategy for an incremental moment in order to avoid error compensations due to the symmetry of some components of the deformation.

### Problem description

The test was designed to obtain a full bending of the beam in 100 steps in which the free edge should complete the 2π angle and touch the clamped edge. In order to do so, we must fulfill the analytical solution $\theta = M \cdot L / E \cdot I$

The beam was defined with a length of 10mm and a width of 0.2mm. The thickness of the shells is set to 0.2mm, to maintain the symmetry of the section and the Inertia.

The material characteristics of the beam are Young's modulus 79577MPa and Poisson's ratio 0.0.

So the resulting moment is 6.6667N·mm

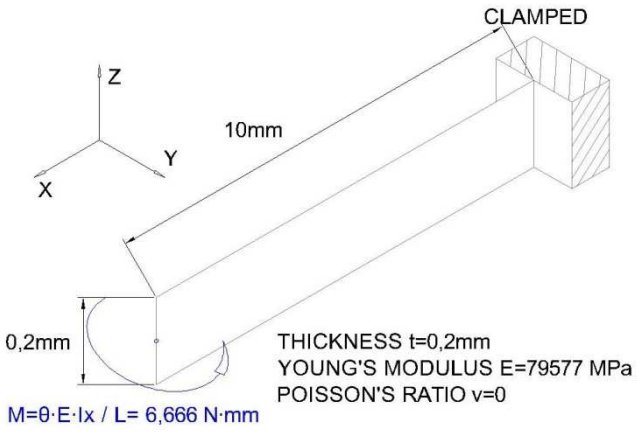


Figure 6 geometry and material properties

A regular mesh of 1 element in the short direction and 12 elements in the long direction was tested as initial mesh. Several refinements in the long direction were made to check the convergence.

*Figure 7*

*The next figure shows the aforementioned mesh*

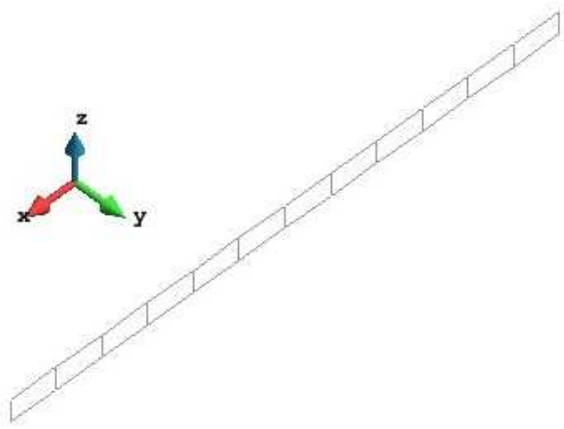


For the triangular element, the same base mesh was used, splitting the quadrilaterals by one diagonal.

The kinematic type analysis was set to Large Displacements, and as mentioned in the before, the total moment was applied in 100 quasi-static steps, in order to check the full curve path for the deformation of the free edge.

## Results

The final step obtained is consistent with the building of the problem, resulting in a circular deformed beam, since the momentum is the only load, and it causes a constant bending deformation.

However, the evolution in time for the z rotation, x and y displacements in the free edge are the magnitudes of interest.

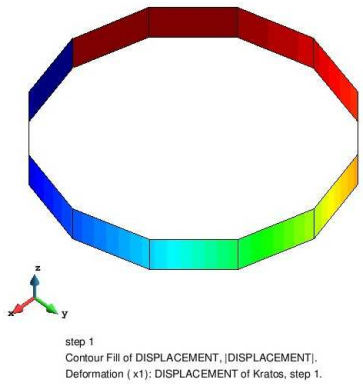


*Figure 8, final deformed state*

Recovering the analytical expression for the rotation, $\theta = M \cdot L / E \cdot I$, and the scheme of the deformation, we can compute also the analytical expression for the displacements. The expressions that read:

$$Ux = r - r \cdot \cos\theta = (L/\theta) \cdot \tan(\theta/2) \cdot \sin\theta$$

$$Uy = L - r \cdot \sin\theta = L - (L/\theta) \cdot \sin\theta$$

The next figures show the evolution and the relative error of the displacement in both x and y directions and the rotation in z direction in the free edge of the beam, for the quadrilateral element and a 1x12 mesh.

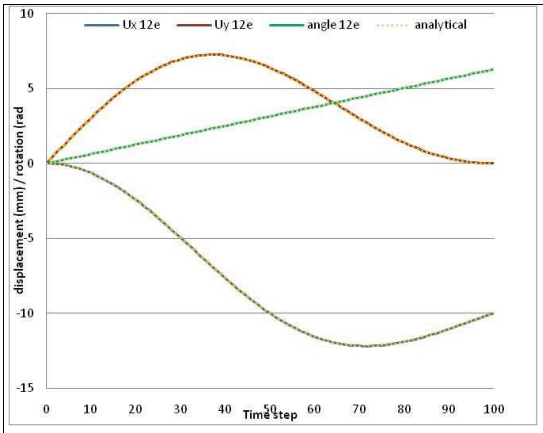


*Figure 9 Ux, Uy and rotZ vs. time step*

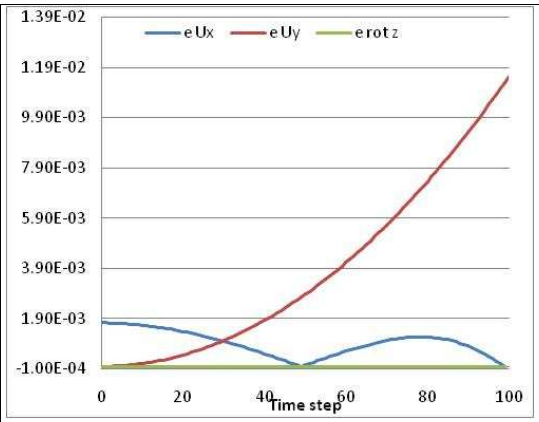


*Figure 10 Absolute value of the relative error vs. time step.*

Even for a quite coarse mesh of 12 elements, the numerical approximation is very accurate, and we need to plot the relative error in order to observe de differences between the numerical and analytical solutions.

For the case of the triangular element, similar figures are obtained.

Analyzing the relative error plot, it can be observed a constant error for the rotation in z of the order of 10^-6. Since the rotation is directly linked to the momentum applied, we are just getting machine precision.

On the other hand, the displacements evolve in a different way. The y displacement starts at zero, and the larger is the momentum applied, the larger becomes the error. On the contrary, the x displacement starts with the larger value, drops to zero at half the momentum (when the free edge gets to the same x position than the clamped edge) and starts another curve to come back to 0 at the end of the loading path.

In order to analyze the evolution of the error as the mesh is refined in a magnitude relevant for the full cycle, the addition of all the absolute values of the relative errors was used. This magnitude was also used later to check the convergence of the element.

The following table shows the evolution of the relative errors with the refinement of the mesh for both triangular and quadrilateral elements.

| | | 12 elements | 24 elements | 48 elements | 96 elements | 192 elements | 384 elements |
|---|---|---|---|---|---|---|---|
| | TRIANGULAR THIN ELEMENTS | | | | | | |
| Ux relative error | Summed | 9.26E-02 | 2.31E-02 | 5.77E-03 | 1.44E-03 | 3.59E-04 | 8.81E-05 |
| | Maximum | 1.74E-03 | 4.34E-04 | 1.08E-04 | 2.70E-05 | 6.71E-06 | 1.72E-06 |
| Uy relative error | Sumemd | 3.89E-01 | 9.69E-02 | 2.43E-02 | 6.16E-03 | 1.63E-03 | 4.92E-04 |
| | Maximum | 1.17E-02 | 3.00E-03 | 8.47E-04 | 3.11E-04 | 1.77E-04 | 1.43E-04 |
| | QUADRILATERAL THICK ELEMENTS | | | | | | |
| Ux relative error | Summed | 9.25E-02 | 2.31E-02 | 5.77E-03 | 1.44E-03 | 3.59E-04 | 8.85E-05 |
| | Maximum | 1.74E-03 | 4.34E-04 | 1.09E-04 | 2.72E-05 | 6.90E-06 | 1.80E-06 |
| Uy relative error | Sumemd | 3.89E-01 | 9.68E-02 | 2.42E-02 | 6.05E-03 | 1.52E-03 | 3.83E-04 |
| | Maximum | 1.15E-02 | 2.89E-03 | 7.38E-04 | 2.02E-04 | 6.77E-05 | 3.42E-05 |

The obtained accuracy is almost the same for both elements.

These results were rearranged in the following plot in order to show the convergence of the elements. Only quadrilateral results are displayed, but triangular elements have similar behavior.

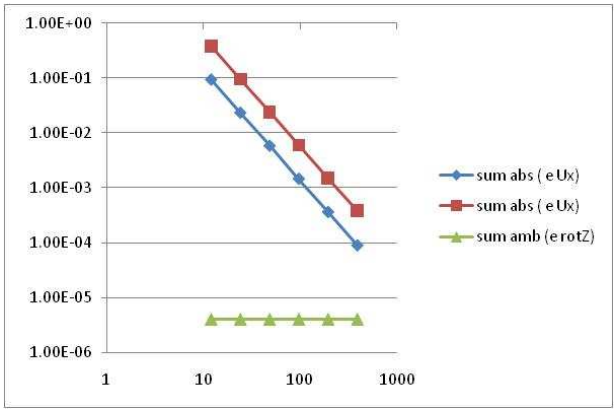


*Figure 11, convergence analysis (abs of relative error vs. n elements log scale) for the quadrilateral thick element.*

The linear slope is almost perfect for both displacement relative errors. For the case of the rotation, the error is a machine precision error, derived from the accuracy of the type of number defined to store the data.

## *4.3. SKEW SENSITIVITY*

The skew sensitivity benchmark is designed to test the performance of the element subjected to skew distortion. This test is especially useful to extend the verification of the element for non regular geometries, since even we test distorted meshes in other benchmarks, other effects different than the angular distortion.

This example can also be compared to known solutions (see L.S.D. Morley, 1963 [18]), what makes it a very useful test for the element. There is also a compendium analysis for various commercial code performed by J. Robinson 1985 [19]

### Problem description

The benchmark consists in a rhomboid plane thin plate simply supported in all the edges. The material characteristics of the plate are Young's modulus 30 MPa, and Poisson's ratio 0.3. An uniform pressure of 1.0 × 10–6 MPa is applied over the entire surface. Static analysis is stated in the type of calculation.

The length of the edges of the rhomboid is fixed to 1.0 m long and 3 different angles are tested 90º, 60º and 30º. The thickness of the plate is 0.01 m, so the ratio thickness/length ratio is 1/100 and consequently shear lock would be significant, and transverse shear deformation should not be significant.

*Figure 12*

*Regular meshes are applied which inherit the angular distortion of the plate's shape. For the triangular mesh, the division of the quadrilateral elements is done by dividing the plate into 4 quadrants and following the direction of the diagonal in each quadrant.*

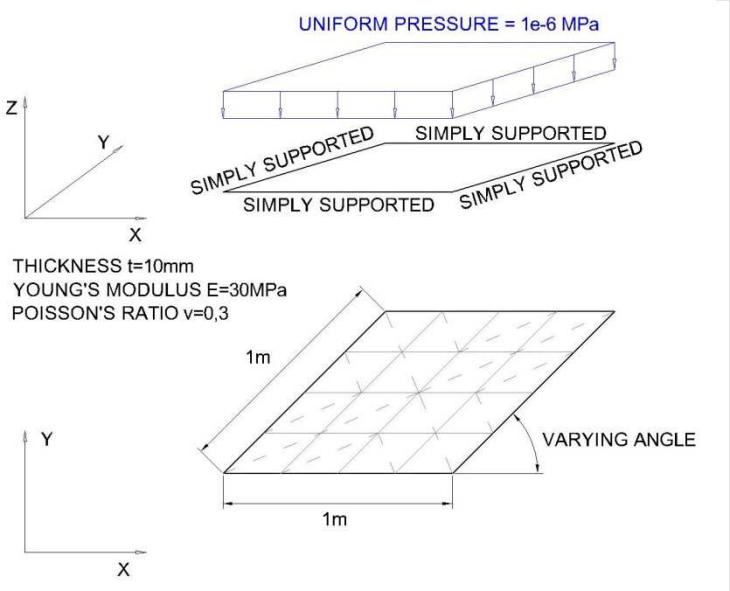


This division enhances the bad shape of the elements in one diagonal direction which is the purpose of the test.

Since the angular definition of plate is sufficient to distort the elements, all the tested meshes are refinement of the following regular meshes attached below.

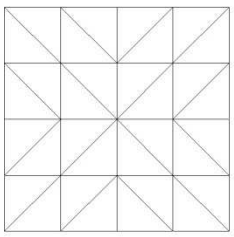

90º mesh

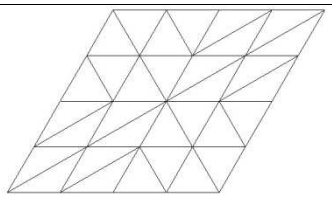

60º mesh

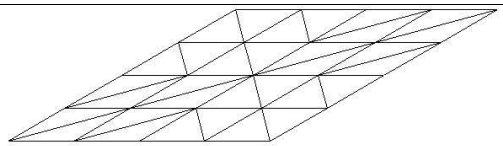

30º mesh

*Figure 13, skew distorted meshes*

The refinements consist in 4x4, 8x8 and 14x14 element regular meshes for the quadrilateral thick element and the division following the diagonal direction for the triangular thin element.

The kinematic type analysis was set to Small Displacements, since it is the case. However, if the Large-displacement theory is to be used, the results would be unchanged in all cases since the strains and rotations remain small.

## Results

The analytical solution based on L.S.D. Morley, 1963 [18], varies with the angle of the plate, so each case can only be compared through the relative errors. The reference value of comparison has been set to the vertical displacement of the center point in the plate, as in the previous test.

The following figure shows a similar distribution of the displacements with different top values at the center of the plate, which coincides with the analytical solution.

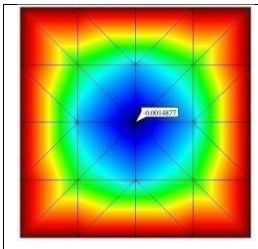

90º mesh

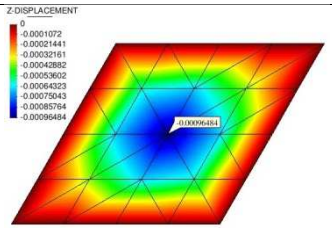


60º mesh

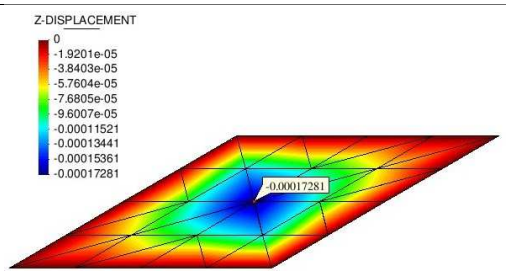


30º mesh

*Figure 14, deflection chart for the 3 skew meshes*

The following tables show the results of the Kratos and again Abaqus elements, since Abaqus was one of the best performers in the skew sensitivity test comparing with other commercial codes results listed in J. Robinson publication aforementioned.

| TRIANGULAR THIN ELEMENTS | | | | | |
|---|---|---|---|---|---|
| | dof | Uz displacement mm | | Error (vs Analytical Solution) | |
| | | S3R Abaqus | Triangular thin Kratos | S3R Abaqus | Triangular thin Kratos |
| 30º | 4x4 | 0.08 | 0.1728 | -46% | 16.76% |
| An.sol. | 8x8 | 0.125 | 0.1583 | -16% | 6.96% |
| 0.148 | 14x14 | 0.148 | 0.1476 | 0% | -0.27% |
| | | | | | |
| 60º | 4x4 | 0.615 | 0.9648 | -34% | 3.52% |
| An.sol. | 8x8 | 0.812 | 0.9396 | -13% | 0.82% |
| 0.932 | 14x14 | 0.913 | 0.9349 | -2% | 0.31% |
| | | | | | |
| 90º | 4x4 | 1.214 | 1.4877 | -18% | 0.66% |
| An.sol. | 8x8 | 1.425 | 1.4811 | -4% | 0.21% |
| 1.478 | 14x14 | 1.462 | 1.4795 | -1% | 0.10% |

.

| QUADRILATERAL THICK ELEMENTS | | | | | |
|---|---|---|---|---|---|
| | dof | Uz displacement ($x10^{-5}$) | | Error (vs Analytical Solution) | |
| | | S4 Abaqus | Quadrilateral thick Kratos | S4 Abaqus | Quadrilateral thick Kratos |
| 30º | 4x4 | 0.131 | 0.1306 | -11% | -11.76% |
| An.sol. | 8x8 | 0.133 | 0.13 | -10% | -12.16% |
| 0.148 | 14x14 | 0.141 | 0.1377 | -5% | -6.96% |
| | | | | | |
| 60º | 4x4 | 0.886 | 0.8851 | -5% | -5.03% |
| An.sol. | 8x8 | 0.91 | 0.9084 | -2% | -2.53% |
| 0.932 | 14x14 | 0.925 | 0.9231 | -1% | -0.95% |
| | | | | | |
| 90º | 4x4 | 1.447 | 1.4461 | -2% | -2.16% |
| An.sol. | 8x8 | 1.474 | 1.4729 | 0% | -0.35% |
| 1.478 | 14x14 | 1.481 | 1.4789 | 0% | 0.06% |

The next plots show the evolution of the relative error versus the dof:

TRIANGULAR THIN ELEMENT (figure 15)

| | | |
|---|---|---|
| 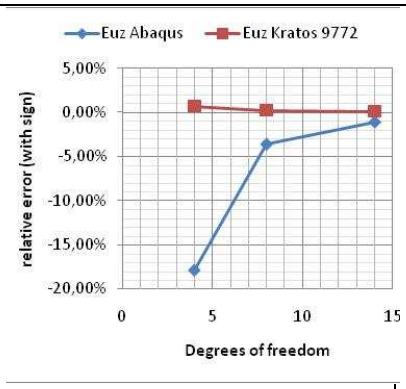 | 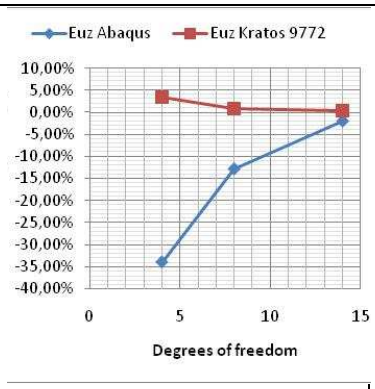 | 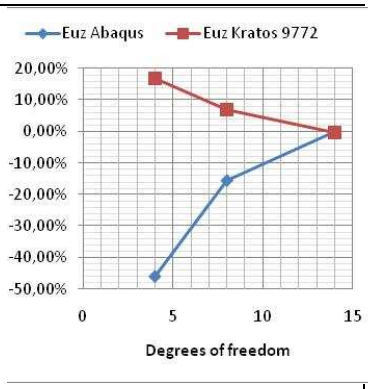 |
| 90º mesh | 60º mesh | 30º mesh |

RECTANGULAR THICK ELEMENT (figure 16)

| | | |
|---|---|---|
| 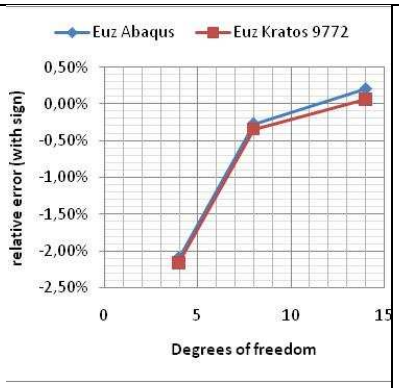 | 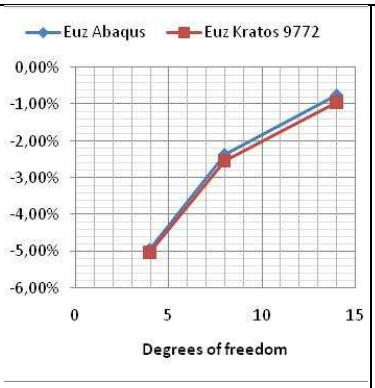 | 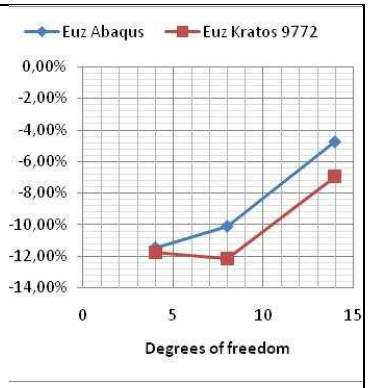 |
| 90º mesh | 60º mesh | 30º mesh |

The Kratos numerical solution converges to the reference one, even though we can see a change of sign in the relative error for 2 of the implemented cases

For this test, we can observe an excellent performance of the triangular thin Kratos element, much better than the element implemented in Abaqus, although for de 30º mesh the larger is the angular distortion; the lesser is the difference among elements. On the other hand, the quadrilateral thick element has a similar performance for 90º and 60º distortions and slightly worst for the 30º distortion.

On the light of the results we can conclude that the element is sensible to skew geometry but the loss of accuracy for this phenomenon, even larger than other elements is acceptable.

## *4.4. TWISTED BEAM*

This problem examines the accuracy of the shell element for large deformations and inextensional bending for warped structures. The warping of the structure turns the bending to mainly torque phenomenon, but other stresses arise. Furthermore, the same cantilever shell beam is subjected to 2 different load cases leading to in-plane or out-of-plane shear. So, this is a quite complete benchmark, for large deformation analysis.

The test was first proposed by MacNeal and Harder (1985) [20], who also provided the analytical solution for the thick twisted beam. The thin twisted beam solution was provided by Simo et al. (1989) [16].

### Problem description

The structure is a cantilever beam twisted 90º about the main center axis which was defined coincident with the x axis. The rotation of the section is constant and anticlockwise advancing from the vertical clamped edge coincident with z axis, to the horizontal free edge parallel to y axis.

The dimensions of the beam are 12.0 in long, 1.1 in wide and for the thickness, two cases were drown, 0.32 in for the thick case and 0.05 in for the thin one.

On the tip of the cantilever, a point load of 1.0 lb is applied. Two different cases are studied. An in-plane load (load in y direction) and an out-plane load (in z direction).

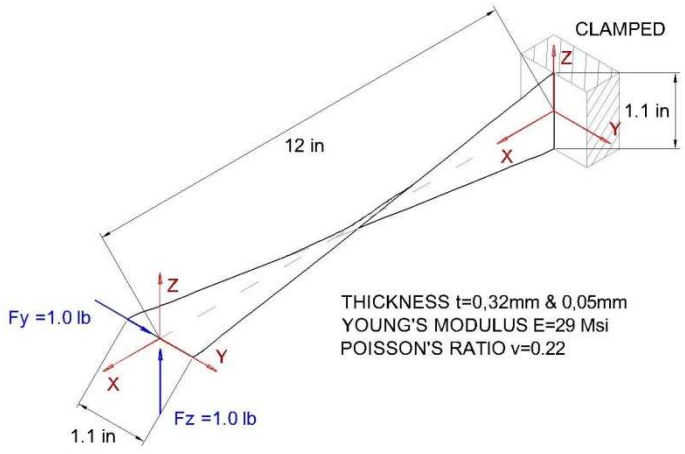


*Figure 17 geometry and material properties*

The material is steel with a Young's modulus of 29.0 Msi and a Poisson's ratio of 0.22.

Since only quadrilateral thick element and triangular thin element are implemented in Kratos up to the date of this work, this benchmark contains 8 different cases, combining the element, the thickness and the direction of the load on the free end.

A set of regular meshes was defined, being the coarsest one a 2 × 12 mesh for the quadrilateral element. This leads to a warp angle of 7.5° per element length. For the triangular element, the coarser mesh consist in a 1 x 6 quadrilateral mesh and each quadrilateral divided in 4 triangles by adding one point in the center. This way, both meshes has the same number of elements and there is no distortion caused by the orientation of the triangles.

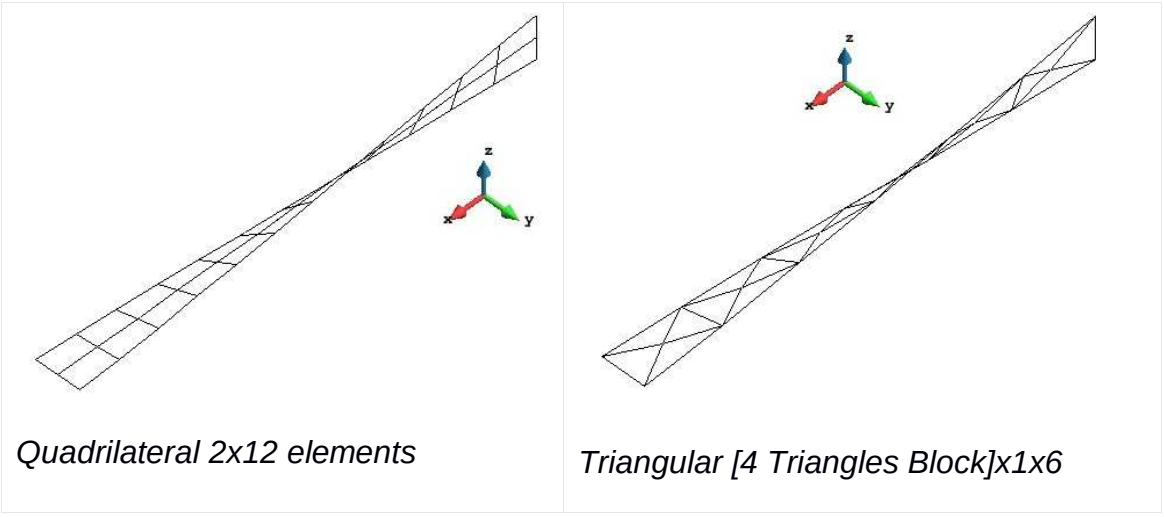


*Quadrilateral 2x12 elements*

*Triangular [4 Triangles Block]x1x6*

*Figure 18 coarser meshes tested (both 24 elements).*

Three refinements of the meshes were used in order to analyze convergence, consisting in 4x24, 8x48 and 16x96 quadrilateral meshes and [4 Triangles Block]x2x12, [4TB]x4x24 and [4TB]x8x48.

In order to implement the coarser triangular mesh, the 1.0 lb point load on the tip, was transformed to 2 point loads of 0.5 lb on the free corners, recovering the tip load for all refined meshes.

The same mesh discretization strategy was used for in-plane, out-plane, 0.32 and 0.05 thickness.

## Results

As advanced, torque is the main bending effect, but the distribution varies strongly if in-plane of out-plane load is applied. While for the in plane (Fy) load, the shell momentum is stronger in the clamed section, for the out-plane case (Fz) it is stronger in the center of the beam. Exactly the opposite applies to the Sxx force, which is the other main stress.

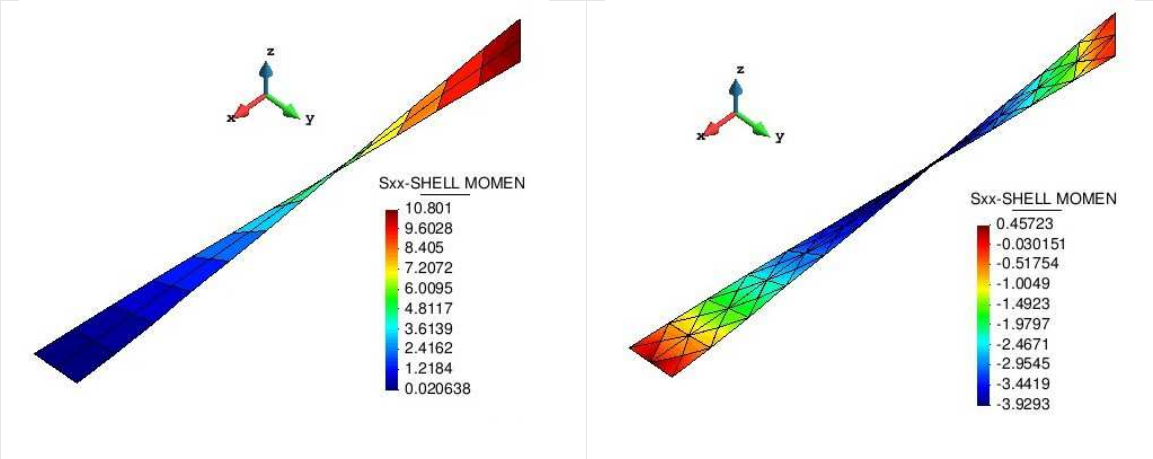


*Figure 19 Sxx moment for Fy and Fz loads*

However, the magnitude of comparison with the reference solution and Abaqus element is the y tip displacement for the case of the Fy load, and the z tip displacement for the case of the Fz one.

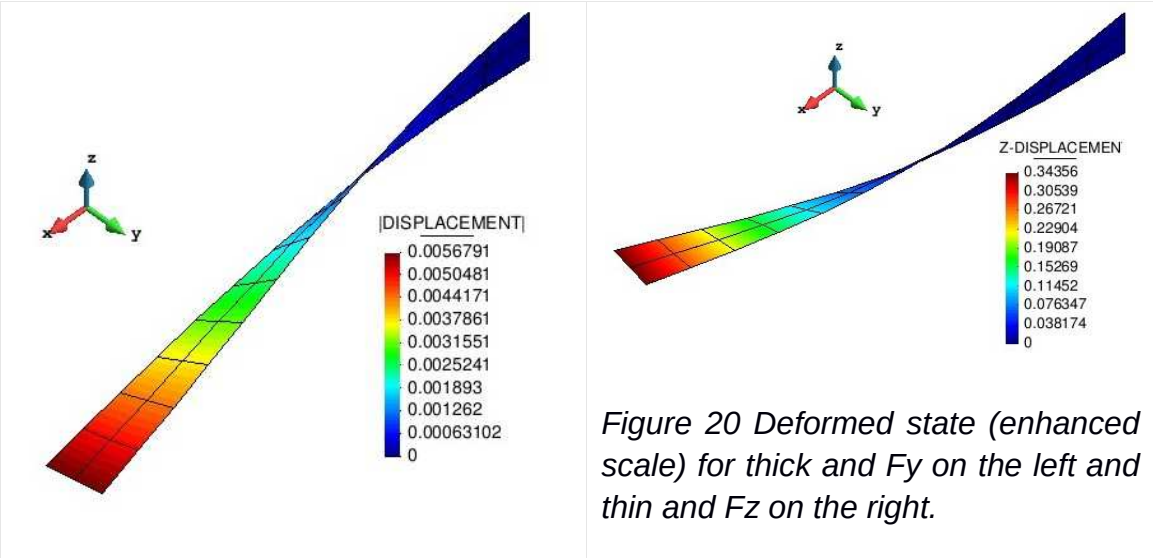


*Figure 20 Deformed state (enhanced scale) for thick and Fy on the left and thin and Fz on the right.*

The following tables contain the results for the proposed problem for the two elements implemented in Kratos and the equivalent elements in the reference software (Abaqus). All the results for the 0.32 versions of the problem are multiplied for $10^{-3}$.

| **QUADRILATERAL THICK ELEMENTS** | | | | | |
|---|---|---|---|---|---|
| FY case | mesh | Uy displacement (in) | | Error (vs Analytical Solution) | |
| | | S4 Abaqus | Quadrilateral thick Kratos | **S4 Abaqus** | **Quadrilateral thick Kratos** |
| Thickness | 2x12 | 5.440 | 5.3942 | **0.29%** | **-0.55%** |
| 0.32 | 4x24 | 5.428 | 5.4104 | **0.07%** | **-0.25%** |
| An.solution (*e-3) | 8x48 | 5.427 | 5.4157 | **0.06%** | **-0.15%** |
| 5.424 | 16x96 | | 5.4176 | | **-0.12%** |
| | | | | | |
| Thickness | 2x12 | 1.391 | 1.3831 | **0.07%** | **-0.50%** |
| 0.05 | 4x24 | 1.388 | 1.3862 | **-0.14%** | **-0.27%** |
| An.solution | 8x48 | 1.388 | 1.3870 | **-0.14%** | **-0.22%** |
| 1.39 | 16x96 | | 1.3873 | | **-0.19%** |
| | | | | | |
| FZ case | mesh | Uy displacement (in) | | Error (vs Analytical Solution) | |
| | | S4 Abaqus | Quadrilateral thick Kratos | **S4 Abaqus** | **Quadrilateral thick Kratos** |
| Thickness | 2x12 | 1.730 | 1.7213 | **-1.37%** | **-1.86%** |
| 0.32 | 4x24 | 1.747 | 1.7438 | **-0.40%** | **-0.58%** |
| An.solution (*e-3) | 8x48 | 1.753 | 1.7510 | **-0.06%** | **-0.17%** |
| 1.754 | 16x96 | | 1.7531 | | **-0.05%** |
| | | | | | |
| Thickness | 2x12 | 0.325 | 0.3436 | **-5.25%** | **0.13%** |
| 0.05 | 4x24 | 0.338 | 0.3430 | **-1.46%** | **-0.03%** |
| An.solution | 8x48 | 0.342 | 0.3430 | **-0.41%** | **-0.03%** |
| 0.3431 | 16x96 | | 0.3430 | | **-0.03%** |

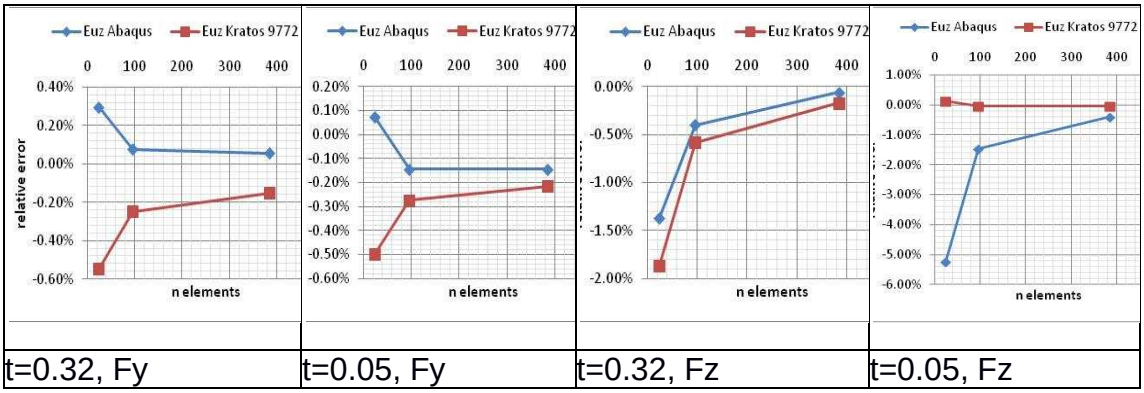


t=0.32, Fy | t=0.05, Fy | t=0.32, Fz | t=0.05, Fz

*Figure 21 Relative error versus n elements comparison for quadrilateral mesh*

| **TRIANGULAR THIN ELEMENTS** | | | | | |
|---|---|---|---|---|---|
| FY case | mesh | Uy displacement (in) | | Error (vs Analytical Solution) | |
| | | S3R Abaqus | Triangular thin Kratos | **S3R Abaqus** | **Triangular thin Kratos** |
| Thickness | [4TB]x1x6 | 5.262 | 5.2862 | **-2.99%** | **-2.54%** |
| 0.32 | [4TB]x2x12 | 5.361 | 5.3791 | **-1.16%** | **-0.83%** |
| An.solution (*e-3) | [4TB]x4x24 | 5.405 | 5.3953 | **-0.35%** | **-0.53%** |
| 5.424 | [4TB]x8x48 | | 5.3984 | | **-0.47%** |
| | | | | | |
| Thickness | [4TB]x1x6 | 1.352 | 0.8839 | **-2.73%** | **-36.41%** |
| 0.05 | [4TB]x2x12 | 1.372 | 1.3139 | **-1.29%** | **-5.47%** |
| An.solution | [4TB]x4x24 | 1.383 | 1.3809 | **-0.50%** | **-0.65%** |
| 1.39 | [4TB]x8x48 | | 1.3865 | | **-0.25%** |
| | | | | | |
| FZ case | mesh | Uy displacement (in) | | Error (vs Analytical Solution) | |
| | | S3R Abaqus | Triangular thin Kratos | **S3R Abaqus** | **Triangular thin Kratos** |
| Thickness | [4TB]x1x6 | 1.400 | 1.5822 | **-20.18%** | **-9.79%** |
| 0.32 | [4TB]x2x12 | 1.581 | 1.6951 | **-9.86%** | **-3.36%** |
| An.solution (*e-3) | [4TB]x4x24 | 1.696 | 1.7346 | **-3.31%** | **-1.11%** |
| 1.754 | [4TB]x8x48 | | 1.7463 | | **-0.44%** |
| | | | | | |
| Thickness | [4TB]x1x6 | 0.325 | 0.2276 | **-5.25%** | **-33.66%** |
| 0.05 | [4TB]x2x12 | 0.338 | 0.3311 | **-1.46%** | **-3.51%** |
| An.solution | [4TB]x4x24 | 0.342 | 0.3422 | **-0.41%** | **-0.25%** |
| 0.3431 | [4TB]x8x48 | | 0.3429 | | **-0.05%** |

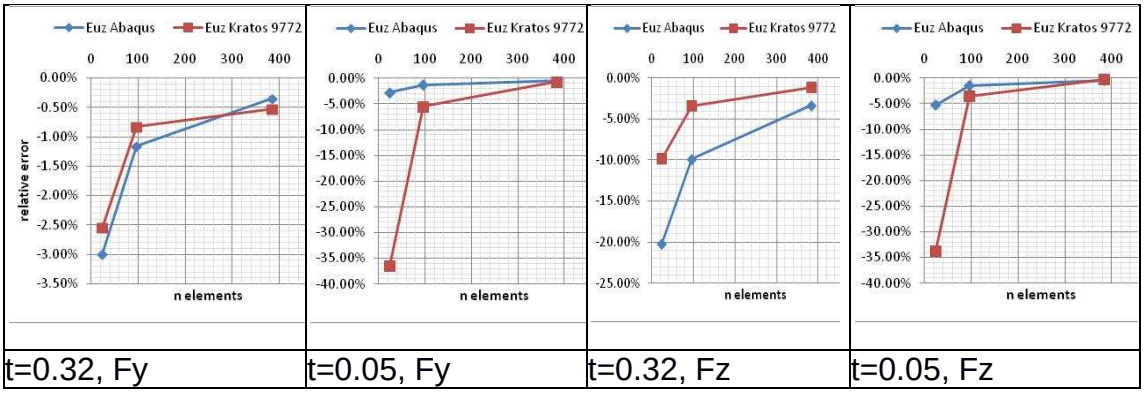


t=0.32, Fy | t=0.05, Fy | t=0.32, Fz | t=0.05, Fz

*Figure 22 Relative error versus n elements comparison for triangular mesh*

The quadrilateral Reissner-Midlin performed well for the 4 cases tested, being the thick out-plane case the only one with a relative error over the 1% for the coarser mesh. Compared with the reference element, the results are slightly worst, but the out of plane thin problem, where Kratos element achieved an extraordinary accuracy.

On the other hand, the triangular Timoshenko element had a poor performance for all the coarser meshes, especially for both cases with a thickness of 0.05 in, with relative errors larger than 30%. However, the error drops drastically by refining the mesh, and at 3$^{rd}$ refinement, all the results have less than a 1% relative error, but the thick out of plane case where it is 1.11%.

To find the cause of this different behavior among the triangular and the quadrilateral elements we must look to distribution of the secondary effects generated for twisted beams.

For the triangular mesh, the shear stresses results jump from element to element. For a shared edge, one element takes a positive value and the adjacent one a negative one. Both extremes compensate the system but this is not physical, and the deformation introduced in each element is the source of the error.

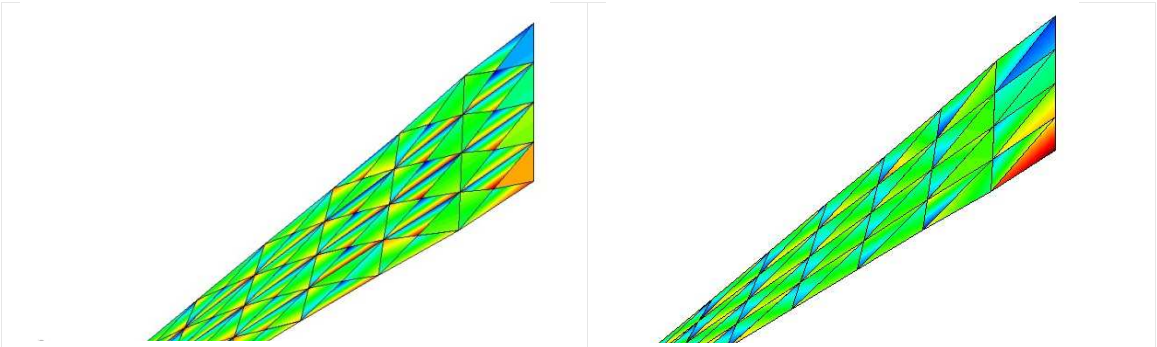

*4TB triangular mesh.* *Diagonal triangular mesh.*

*Figure 23 Zoom of the* Syy force *distribution* for Fz case

Testing another triangular mesh consisting in dividing the quadrilaterals by 1 diagonal, rather than splitting it in 4 triangles adding one point in the center, this effect is reduced but not suppressed. Consequently the results improve but still need 2 refinements to achieve less than 1% relative error.

The CR formulation is specifically sensitive to this effect, since as stated in the theory, displacements and rotations may be arbitrarily large, but deformations

must be small. A discontinuous distribution of the stresses enhances the deformation of one element and the opposite deformation in the adjacent one. On the contrary, a uniform distribution, allows enhance the displacement and rotation of the element over the deformation.

Even with this problem, after 2 refinements of the mesh the obtained accuracy is acceptable, and on the order of the referent elements. The accuracy is slightly worse for the in-plane load, but better in the out of plane loading, were Kratos elements capture faster the in-plane bending at the built-end.

The next figures show the convergence for the 4 cases and both elements

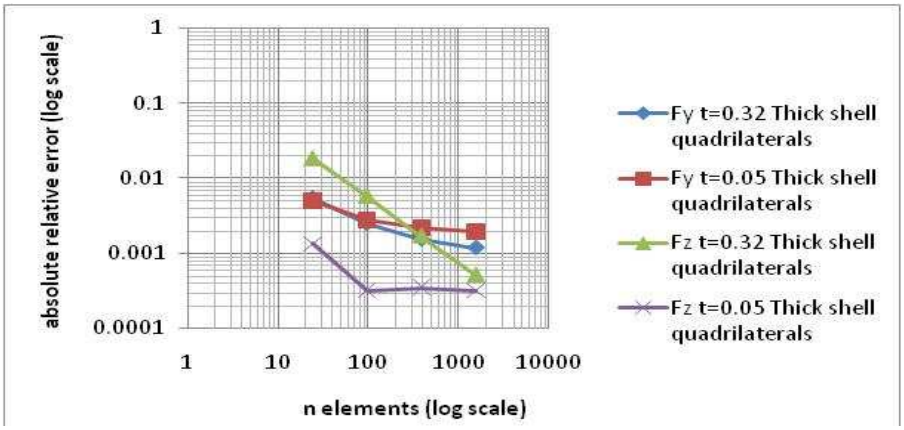


*Figure 24 convergence analysis (abs relative error vs. n elements log scale)*

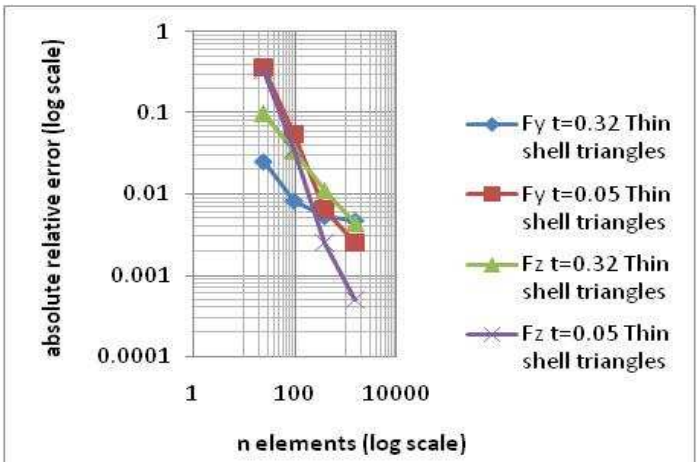


It can be seen that although the results in the triangular case had a worst start, the slope of convergence is larger, and for 1536 elements the order of magnitude is the same. We can also see that the slope turns almost horizontal for the quadrilateral element, which is not a good behavior, since an early peak of accuracy is reached, not allowing more precise calculations.

## *4.5. PINCHED CYLINDER*

The pinched cylinder with a diaphragm is one of the most severe tests for both inextensional bending modes and complex membrane states. It is specially demanding for shell elements, and as a consequence, most of the Mindlin elements, accounting for shear deformation do not converge efficiently in this problem, except for Kirchhoff formulations.

As stated in [21] T. Belytschko 1985, an element that passes this test will also perform well if the boundary conditions are simplified to free ends. It is therefore sufficient to present only the cylinder with diaphragms.

Furthermore, this example is especially useful because comparison can be made with known solutions (see [22] G.Lindberg et al., 1969).

### Problem description

The benchmark consists in a cylinder with a rigid diaphragm in each circular base, subjected to two diametrically opposite point loads in the center.

Exploiting the symmetry of the problem, only 1/8 of the cylinder is modeled with 3 of the boundaries with symmetry B.C. and the in the forth one (the end of the cylinder), diaphragm B.C. Uy=Uz=Rx=0 are applied.

*Figure 25*

*The following figure collects the geometry and material properties used for the test. The model is built in a self-consistent set of units, and because of this they are not written since any self-consistent set can be used.*

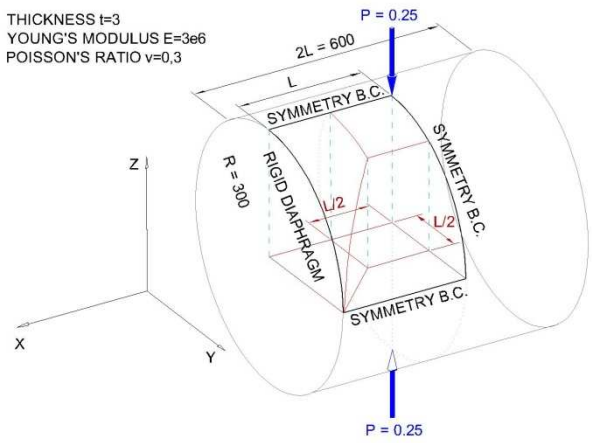


The thickness of the cylinder is 1/100 of its radius, so the structure can be considered a thin shell.

Three different quadrilateral and triangular meshes are used in the test, being the triangular ones just the division of the quadrilateral elements. The 2 additional meshed have the purpose of checking the distortion sensitivity of the elements and are designed to fulfill the common needs of refine and improve accuracy to analyze local effects.

The 1st mesh is regular with an uniform distribution of 5x5 elements, which leads to 36 nodes and 216 degrees of freedom (dof from now on).

In order to build the 2nd mesh, the starting point is the projection of the 1/8 of the cylinder into the XY plane. In the resulting rectangle, a smaller rectangle is created from the vertex of the projection of the applied load, taking 1/2 of the length in both edges. Then a diagonal edge is added to divide the “L” shaped polygon into two quadrilaterals. The 3 resulting quadrilaterals are projected back to the cylinder (in z direction) and an 8x8 element mesh is applied to the smaller surface, and a 4x8 mesh to the other 2 surfaces. This mesh has 894 dof.

The 3rd mesh has the same process but 1/5 of the length is taken for the edges of the smaller rectangle.

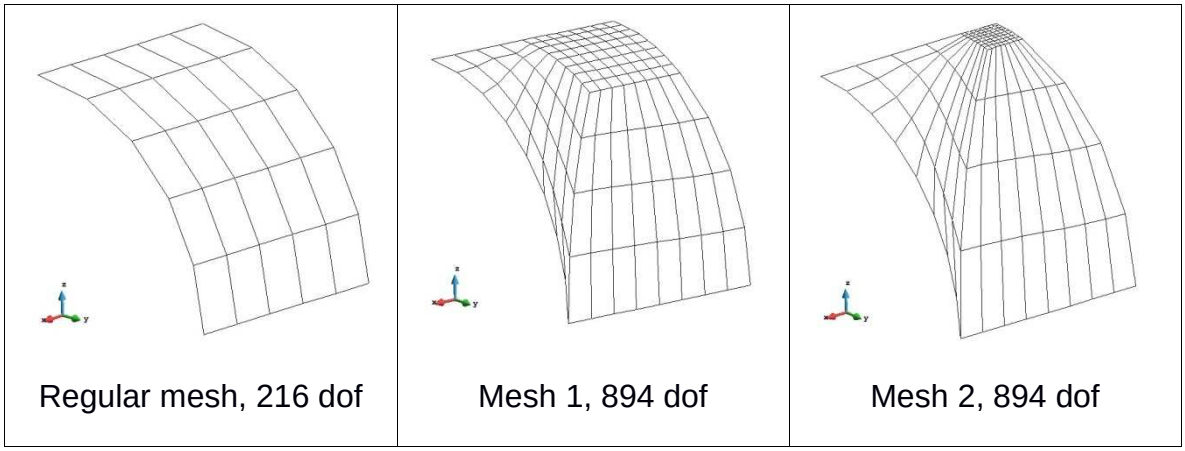


*Figure 26. Meshes for pinched cylinder test*

Some additional meshes have been tested, been just a refinement of the 3 described above using twice the elements of the previous mesh. The results would refer to regular mesh, mesh 1 or mesh 2 and the dof in the mesh refinement.

The kinematic type analysis was set to Small Displacements, since it is the case. However, if the Large-displacement theory is to be used, the results would be unchanged in all cases since the strains and rotations remain small.

## Results

The analytical solution based on Flügge's (1973) series solution and that can be checked in Lindberg et al., states that the radial displacement at the point where the pinching load is applied is equal to 0.1825 × 10–4.

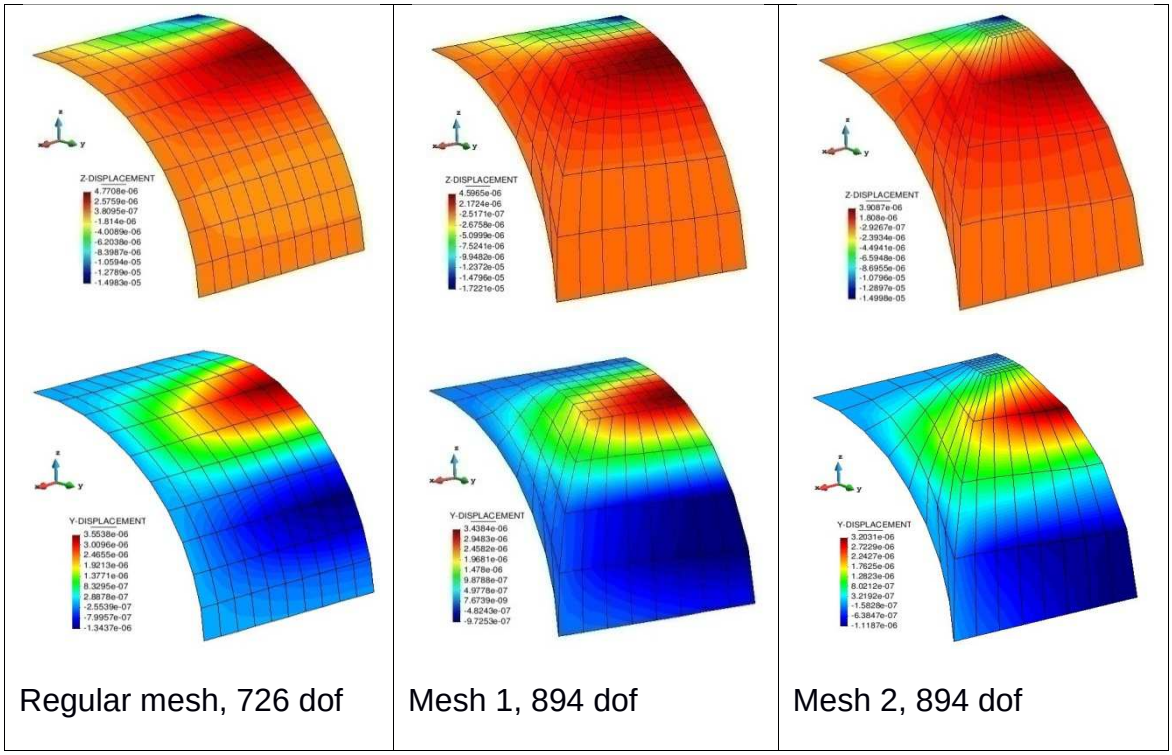


*Figure 27 Z and Y displacement for quadrilateral thick element of Kratos solver.*

As shown in the figures and latter on the tables of results, distorting the mesh does not have a great impact in the result. For a roughly equal number of dof, we obtain slightly worse results as larger is the distortion, but the loss of accuracy is not significant. The same analysis can be applied to triangular thin elements, as shown below.

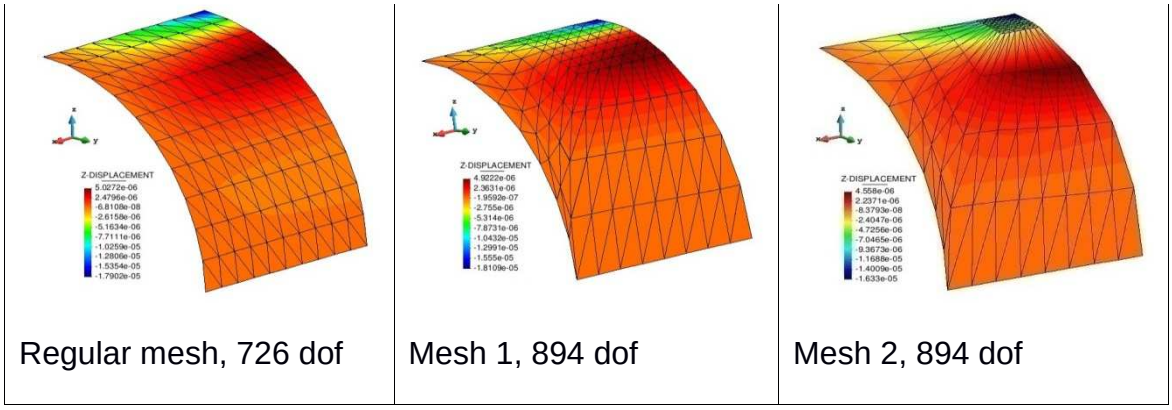


*Figure 28 Z and Y displacement for triangular thin element of Kratos solver.*

The following tables show the results of the Kratos and Abaqus elements, in order to put into perspective the performance of the implemented elements.

| TRIANGULAR THIN ELEMENTS | | | | | |
|---|---|---|---|---|---|
| | dof | Uz displacement ($x10^{-5}$) | | Error (Analytical Solution 1,825e-5) | |
| | | S3R Abaqus | Triangular thin Kratos | S3R Abaqus | Triangular thin Kratos |
| Regular mesh | 216 | 0.635 | 1.3705 | -65% | -24.90% |
| | 726 | 1.328 | 1.7902 | -27% | -1.91% |
| | 2646 | 1.674 | 1.855 | -8% | 1.64% |
| | 12774 | | 1.8417 | | 0.92% |
| | 50118 | | 1.833 | | 0.44% |
| Mesh 1 | 894 | 1.565 | 1.8109 | -14% | -0.77% |
| | 3318 | 1.763 | 1.827 | -3% | 0.11% |
| Mesh 2 | 894 | 1.27 | 1.605 | -30% | -12.05% |
| | 3318 | 1.654 | 1.829 | -9% | 0.22% |

In this case, convergence towards the reference solution can be observed, but the 2646 elements regular mesh were the relative error changes of sign has almost the same error than the previous coarser mesh.

Two additional refinements for the regular mesh were calculated in order to ensure that the element is really converging and does not keep increasing. As shown in the table, for the 2 refinements of the mesh, the relative error keeps reducing, so the numerical solution is converging towards the analytical one. At the end of the case a convergence plot is attached.

| QUADRILATERAL THICK ELEMENTS | | | | | |
|---|---|---|---|---|---|
| | dof | Uz displacement ($x10^{-5}$) | | Error (Analytical Solution 1,825e-5) | |
| | | S4 Abaqus | Quadrilateral thick Kratos | S4 Abaqus | Quadrilateral thick Kratos |
| Regular mesh | 216 | 0.951 | 0.905 | -48% | -50.41% |
| | 726 | 1.519 | 1.498 | -17% | -17.92% |
| | 2646 | 1.75 | 1.745 | -4% | -4.38% |
| Mesh 1 | 894 | 1.687 | 1.7221 | -8% | -5.64% |
| | 3318 | 1.814 | 1.8121 | -1% | -0.71% |
| Mesh 2 | 894 | 1.454 | 1.4998 | -20% | -17.82% |
| | 3318 | 1.777 | 1.7496 | -3% | -4.13% |

The next plots show the evolution of the relative error versus the dof:

TRIANGULAR THIN ELEMENT (figure 29)

| | | |
|---|---|---|
| 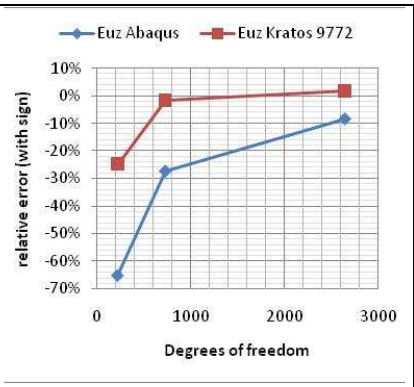 | 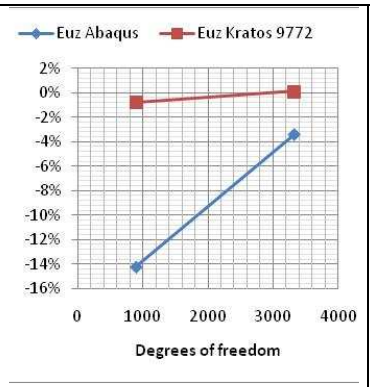 | 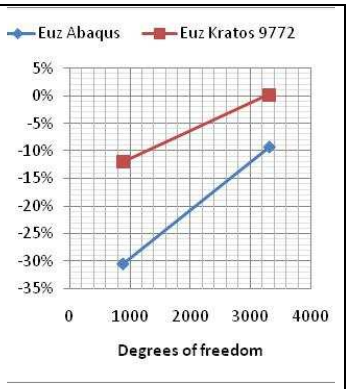 |
| Regular mesh | Mesh 1 | Mesh 2 |

RECTANGULAR THICK ELEMENT (figure 30)

| | | |
|---|---|---|
| 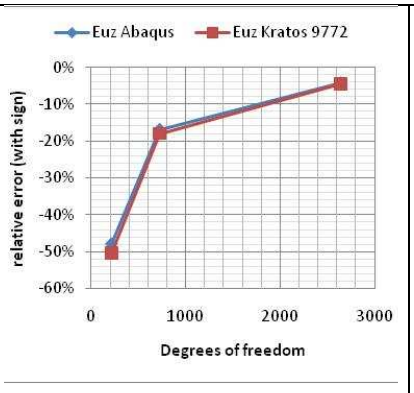 | 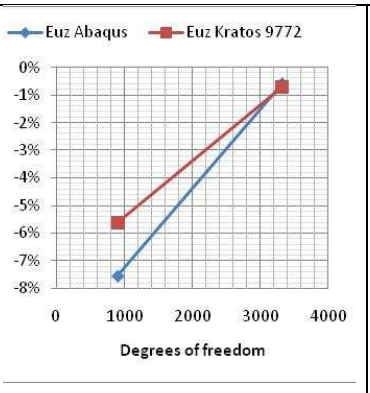 | 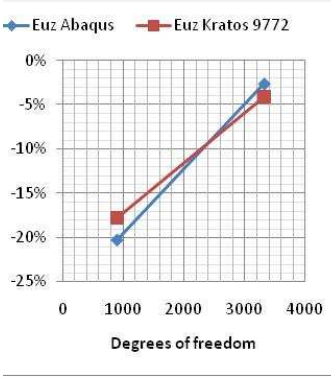 |
| Regular mesh | Mesh 1 | Mesh 2 |

Comparing the results of the CR triangular thin element implemented in Kratos with an analog shell element, as is the case of S3R of Abaqus, shows that the results have much greater accuracy. However, we can see that at the test with regular mesh and 2646 dof, the obtained value exceeded the analytical solution, even the previous results were not.

On the other hand, analyzing the results of quadrilateral thick elements tested, similar accuracy can be observed, even slightly worst for the thick CR element than for the S4 element implemented in Abaqus.

The next figure contains the convergence analysis of the triangular thin element and regular mesh. An irregularity of the slope arises because the non absolute relative error changes the sign after second refinement, but even then the solution keeps converging. The slope of convergence is larger the coarser is the mesh, and then it stabilizes at an almost constant slope.

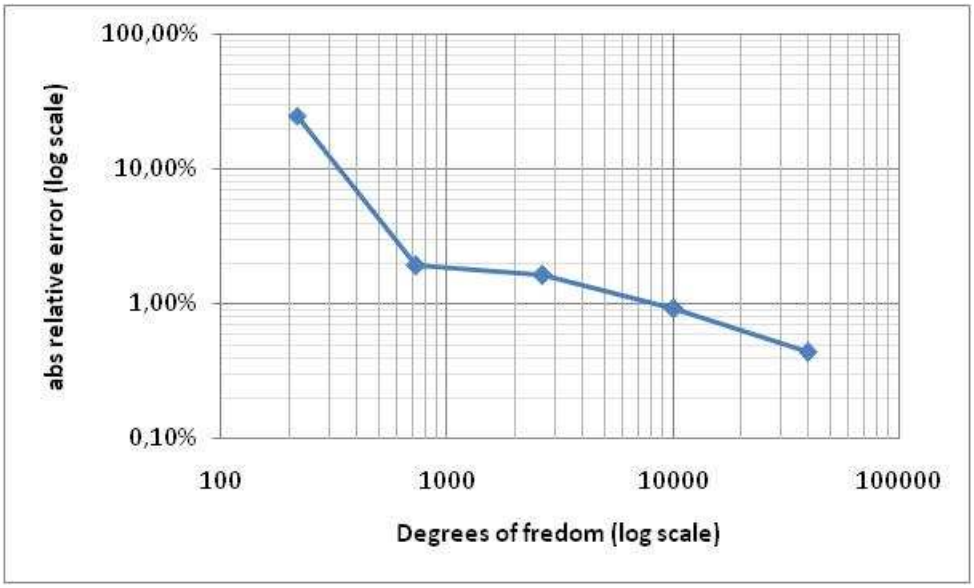


*Figure 31, convergence analysis (abs of relative error vs. dof, log scale)*

## *4.6. SCORDELIS-LO ROOF (THE BARREL VAULT ROOF PROBLEM)*

The pinched last linear test performed is the Sordelis-Lo Roof problem. It is also a demanding test for both inextensional bending modes and complex membrane states. As example on the early publications there is not agreement about the converging reference solution.

The first mention to the problem was by A. C. Scordelis and K. S. Lo. 1964 [23], but several publications argue about the method and the material properties used. Among the publications are D. G. Ashwell, R. H. Gallagher, Editors, 1976. [24], T. J. R.Hughes, R. L. Taylor, and W. Kanoknukulchai, 1977. [25] , R.H. MacNeal, R. L. Harder. 1985. [20] or T. Belytschko. 1986. [26]

Main discussion is that Scordelis work was based on the work of Gibson , in which the shell geometry is shallow, however the load components were calculated as if the shell was deep. However, discussion on the Poisson's ratio and Young Modulus can be found.

The present work uses the standardization used in the last decade of 20$^{th}$ century discarding the value of 0.3086 length units as the mid side vertical displacement. The reference values stated in all recent publications are 0.0 Poisson's ratio, 4.32e8 Young Modulus and 0.3024 as solution.

### Problem description

In this example, a single span, cylindrical barrel vault roof is analyzed for gravity loads. The deeply arched roof is supported only by diaphragms (Ux=Uy=Rz=0 B.C.) at its curved edges, leaving the straight edges free.

The curvature of the roof is a radius of 25, forming a 40º towards both sides of the XZ plane which contains the line with the upper points of the roof. The roof spans longitudinally 50 unit length between supports, and its thickness is 0.25 units.

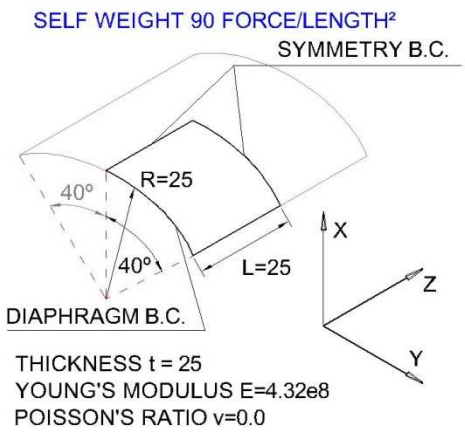


*Figure 32 graphical description* for *Scordelis-Lo roof problem*

The symmetry of the problem allows us to model only 1/4 of the roof applying symmetry B.C. to intersections with XY and XZ planes as seen in the figure.

As advanced in the introduction, material properties modeled are 0.0 Poisson's ratio, 4.32e8 Young Modulus, in agreement with latest normalization of the problem.

Three different meshes are used in the test. The quadrilateral one is a regular distribution of elements and the 2 triangular ones are the division of this quadrilateral mesh following both diagonals.

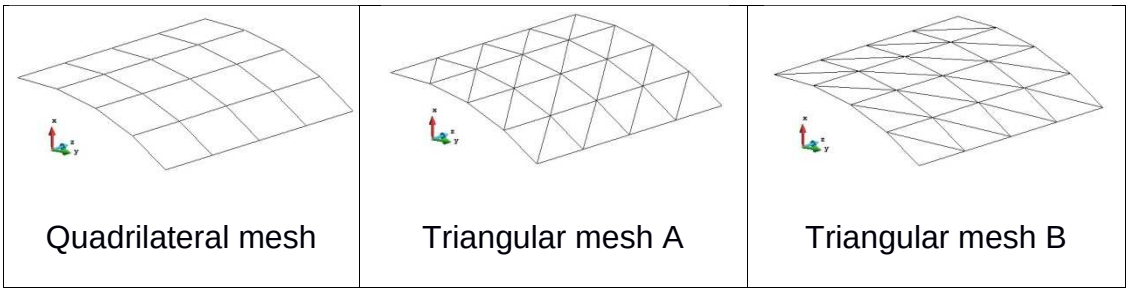


*Figure 33. Meshes for Scordelis-Lo roof*

The coarser mesh consist in a 2x2 mesh, and refinement generally consist in doubling the number of elements per side, however, in order to compare with all the reference element, a 6x6 and a 10x10 mesh were used for quadrilaterals, while only a 20x20 extra mesh was tested for the triangular cases. The 20x20 mesh Is the finer one tested for all the cases.

As all the previous linear cases (but the quasi-static one) the kinematic type analysis was set to Small Displacements.

## Results

The result of the barrel vault problem is not a straight forward one. As consequence of the of the complex stress state, the gravity load makes the central part of the roof to lift slightly while the free edge and all lower part of the roof drops as expected.

The reference magnitude is the deflection of the central point of the free edge, and the referent solution is 0.3024 as almost all the recent publications.

Even the coarser meshes are capable of capturing the general behavior, although they do it with considerable error. As example the next figure show the final deformation state for all 4x4 meshes.

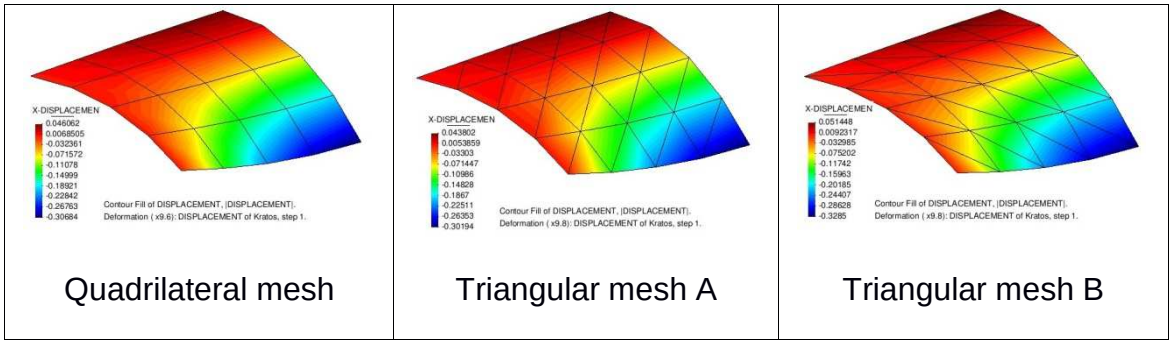


*Figure 34. Numerical results for Kratos coarse meshes*

The following tables contain the results of the Kratos and Xfinas elements, in order to put into perspective the performance of the implemented elements.

| | | **TIP Y DISPLACEMENT** | | **RELATIVE ERROR** | |
|---|---|---|---|---|---|
| Analytical solution | | | 0.3024 | | |
| | mesh | Xshell41 | Triangular thin Kratos | **Xshell41** | **Triangular thin Kratos** |
| Quadrilateral | 2x2 | | 0.3954 | | **30.74%** |
| | 4x4 | 0.312 | 0.3068 | **3.30%** | **1.47%** |
| | 6x6 | 0.305 | 0.3019 | **0.80%** | **-0.15%** |
| | 8x8 | 0.303 | 0.3011 | **0.10%** | **-0.42%** |
| | 10x10 | 0.302 | 0.3009 | **-0.10%** | **-0.49%** |
| | 16x16 | | 0.3009 | | **-0.51%** |
| | 32x32 | | 0.3010 | | **-0.46%** |
| | 64X64 | | 0.3012 | | **-0.39%** |
| | 128X128 | | 0.3014 | | **-0.34%** |
| | | Xshell31 | Triangular thin Kratos | **Xshell31** | **Triangular thin Kratos** |
| Triangular Mesh A | 2x2 | 0.300 | 0.3439 | **-0.80%** | **13.73%** |
| | 4x4 | 0.277 | 0.3019 | **-8.30%** | **-0.15%** |
| | 8x8 | 0.292 | 0.3003 | **-3.30%** | **-0.71%** |
| | 16x16 | 0.299 | 0.3004 | **-1.10%** | **-0.66%** |
| | 20x20 | 0.298 | 0.3005 | **-1.40%** | **-0.64%** |
| | | | | | |
| Triangular Mesh B | 2x2 | 0.298 | 0.4640 | **-1.40%** | **53.43%** |
| | 4x4 | 0.275 | 0.3285 | **-8.90%** | **8.63%** |
| | 8x8 | 0.292 | 0.3069 | **-3.60%** | **1.48%** |
| | 16x16 | 0.298 | 0.3021 | **-1.50%** | **-0.10%** |
| | 20x20 | 0.299 | 0.3015 | **-1.20%** | **-0.29%** |

The next plots show the evolution of the relative error versus the elements in one direction.

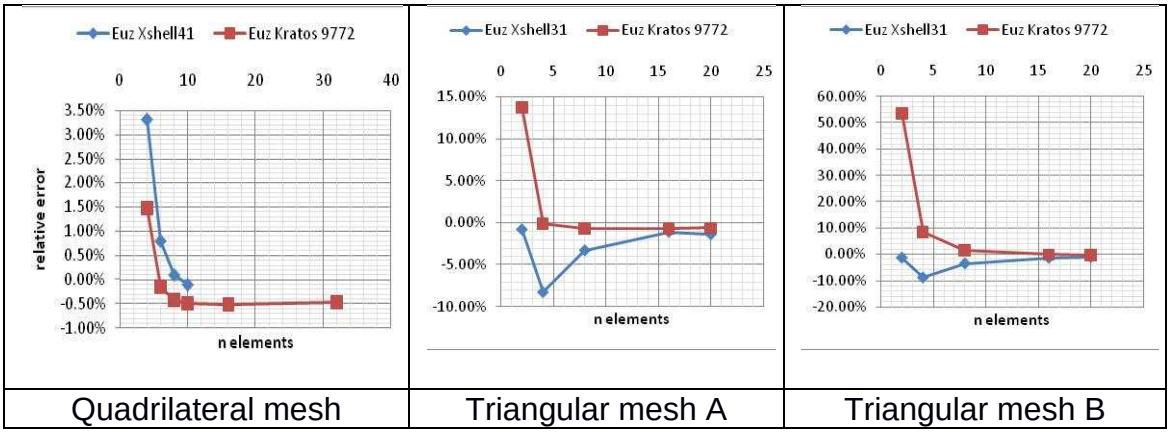


| Quadrilateral mesh | Triangular mesh A | Triangular mesh B |
|---|---|---|

*Figure 35. Relative error for all Kratos elements*

Regarding the Kratos results, it can be observed a common behavior of the elements with all the previous cases. It consist in a really fast starting convergence curve to the reference solution, then the error value of the numerical solutions surpasses the reference one (changes sign), and after reaching a local maximum for the relative error on the opposite sign of the initial one, another much slower convergence curve starts.

Comparing the results of the CR triangular thin element implemented in Kratos with an analog 3 points elements of Xfinas, and neglecting the 2x2 mesh were Xfinas is obtaining a lucky initial value, leads to realization Kratos results show greater accuracy.

On the other hand, analyzing the results of quadrilateral thick elements tested, it can observed a faster convergence until the solution surpasses the reference value, but then several refined meshes obtain results close to 0,5% relative error until the reverse convergence curve starts.

It must be said that the quadrilateral Kratos element is a Reissner-Midlin formulation, but the thickness/span ratio is 1/100 so a Kirchhoff element would perform better.

The following convergence analysis shows neatly the two steps convergence displayed for the elements in various cases. In this case the maximum after the change of sign of the relative error is extraordinarily high and the second convergence step is specially slow, so was the case were more refinements were performed in order to ensure the convergence of the elements.

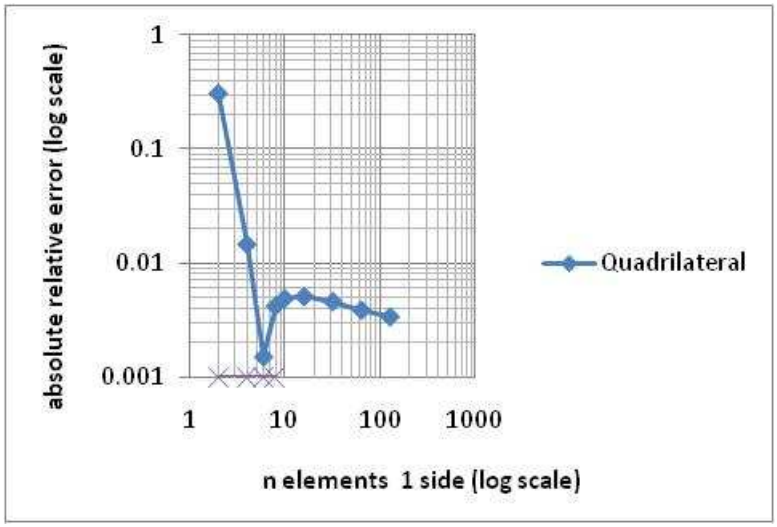


*Figure 36, convergence analysis (abs of relative error vs. n elements, log scale)*

# 5. NON LINEAR STATIC ANALYSIS OF ISOTROPIC SHELL ELEMENT

## *5.1. ELASTIC LARGE DEFLECTION RESPONSE OF A Z-SHAPED CANTILEVER UNDER AN END LOAD*

This is a test recommended by the National Agency for Finite Element Methods and Standards (U.K.): Test 3DNLG-1 from NAFEMS Publication R0024 [27]. Since the published results of this NAFEMS were made with Abaqus software this is the verification result versus which the Kratos results were compared.

In this non-linear test, the incremental end load makes bend the cantilever in an inversely exponential rate, and the magnitude of interest is the tip deflection produced in the end edge and its evolution in time.

### Problem description

The benchmark consist in a z-shaped cantilever with 3 horizontal plates of 60x20mm separated by 30mm in vertical and 60mm in horizontal, and a central sloping plate, of 60x20mm in plan that joins the former plates. The material characteristics of the plate are Young's modulus 2.05e5 MPa and Poisson's ratio 0.3.

Non-linear, large displacements and quasi static analysis is stated in the type of calculation. The cantilever is clamped in one edge, and in the other a total end load of 4000 N is applied in 100 equal time intervals. An uniform pressure of 1.0 × 10–6 is applied over the entire surface.

*Figure 37*

*The following figure displays the geometry of the benchmark.*

*Since 1 element width meshes were used, single loads were applied on the free edge.*

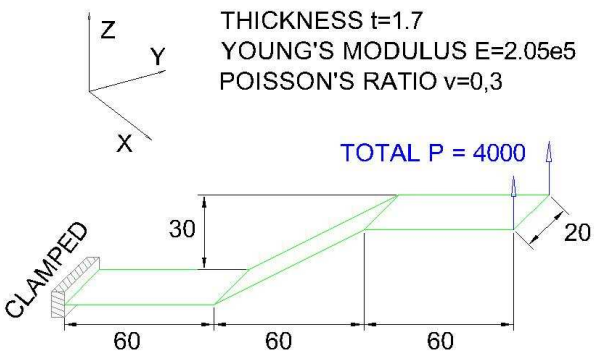

A regular mesh of 1 element in the short direction and 72 elements in the long one is defined. This results in 24 elements of 2.5mm in plan view for plate forming the cantilever.

*Figure 38*

*The next figure shows the aforementioned mesh*

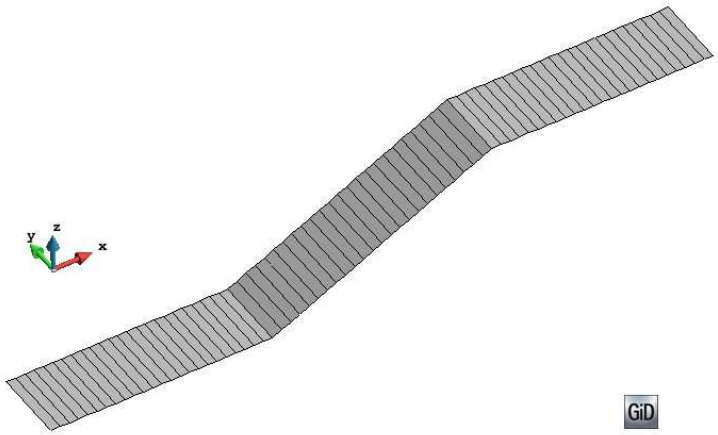


In the NAFEMS publication the triangular element is not tested, but since in Kratos the reduced integration is only implemented for the triangular element, the current work includes a mesh consisting in the splitting of the rectangles by the diagonal.

## Results

*Figure 39*

*The following figure shows the final step for the z deformation of the cantilever.*

*The scale of the deformation is x1 and we can observe the large deformation of the proposed benchmark.*

*In order to check the convergence of the element to this test, and also to verify the results of the reference solution, two refinements of the mesh were implemented, and 2 coarser mesh were also tested. Since the results are very close, only the divergence analysis of the tip deflection will be displayed.*

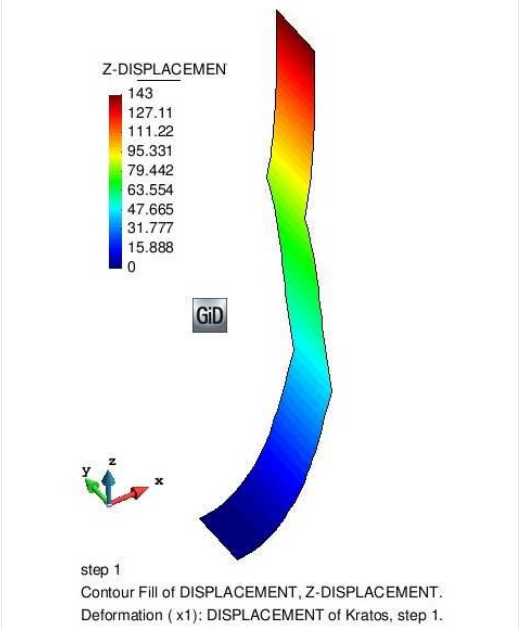

Apart from the final deformational step, also the evolution in time is of interest in a quasistatic nonlinear analysis.

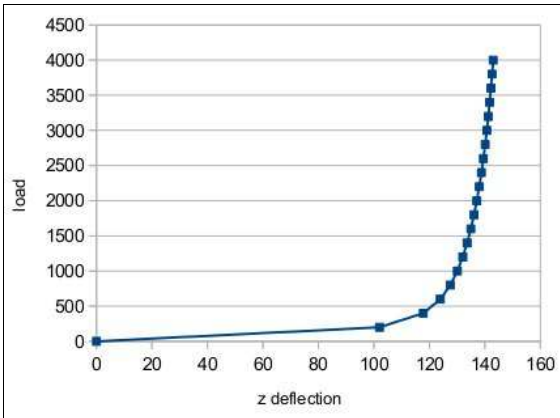


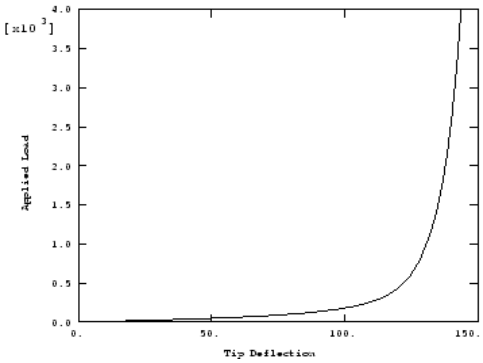


| Kratos numerical solution | Reference numerical solution NAFEMS |
|---|---|

*Figure 40 Maximum deflection* for 100 time steps in the case of Kratos and the reference solution from the NAFEMS publications.

The numerical comparison with the NAFEMS reference is attached below. For the quadrilateral thick Kratos elements, a 8000 steps calculation was performed. On the other hand, since there is no triangular element reference, the triangular results for applied load 104.5 and 1263 were interpolated from a 100 time step calculation.

**RESULTS FOR TIP Z DEFLETION**

| All quadrilateral meshes 1x72 elements and the tiangular one splited by the diagonal | APPLIED LOAD | | |
|---|---|---|---|
| | 104.5 | 1263.0 | 4000.0 |
| NAFEMS thick (S4 Abaqus ) | **80.42** | **133.1** | **143.5** |
| Quadrilateral thick Kratos | **78.96** | **132.34** | **142.68** |
| Relative difference | **-1.81%** | **-0.57%** | **-0.57%** |
| NAFEMS thin (S4R Abaqus ) | **80.42** | **133.1** | **143.5** |
| Triangular thin Kratos | **78.83** | **132.22** | **142.88** |
| Relative difference | **-1.98%** | **-0.66%** | **-0.43%** |

The obtained results have less than a 2% of difference respect the reference solution. However, the reference solution is not an analytical one.

The obtained solution defends also on the time discretization, and for the purposes of the current benchmark, a 100 steps time discretization is enough to check the convergence, especially when the results differ in less than a 1% from the 8000 time steps needed to compare with the NAFEMS solution.

Hence, in order to perform the convergence analysis, the solution for a 1x300 Kratos elements mesh and 100 steps in time was set as the reference solution. The 1x18, 1x36, 1x72, 1x150 I 1x300 where the meshes computed with results of 142.68, 123.92, 142.99, 143.02 and 143.02 respectively.

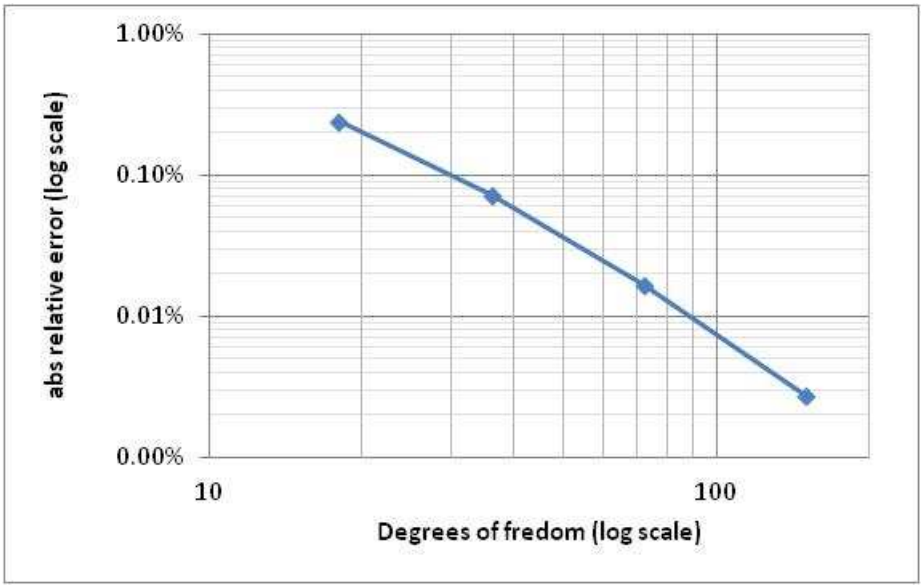


*Figure 41, convergence analysis (abs of relative error vs. n dof, log scale) for the quadrilateral thick element.*

## *5.2. LARGE ELASTIC DEFLECTION OF A PINCHED HEMISPHERICAL SHELL*

This test also belongs to the NAFEMS Publication R0024 [27] Its reference number is test 3DNLG-9.

This non-linear test consists in as hemispherical shell with a circular hole at its pole, which is loaded with two compressive and two tensile forces applied in alternating mode every 90 degrees along the lower free boundary of the shell.

The hemispherical shape leads to an increasing resistance to deformation that is responsible of the non-linear behavior.

### Problem description

The radius of the hemispherical shell is 10 m, its thickness is 0.040 m and the upper hole forms an angle of 18º between the z axis and any line joining the limit of the hole with the center of the hemisphere.

Taking advantage of the symmetry of the problem, only 1/4 of the hemisphere is modeled, with the 2 lateral the boundaries with symmetry B.C. and the other 2 (upper and lower) free, as stated by the problem description.

*Figure 42*

*The following figure shows the geometry and material properties used for the test. The model is built in a self-consistent set of units.*

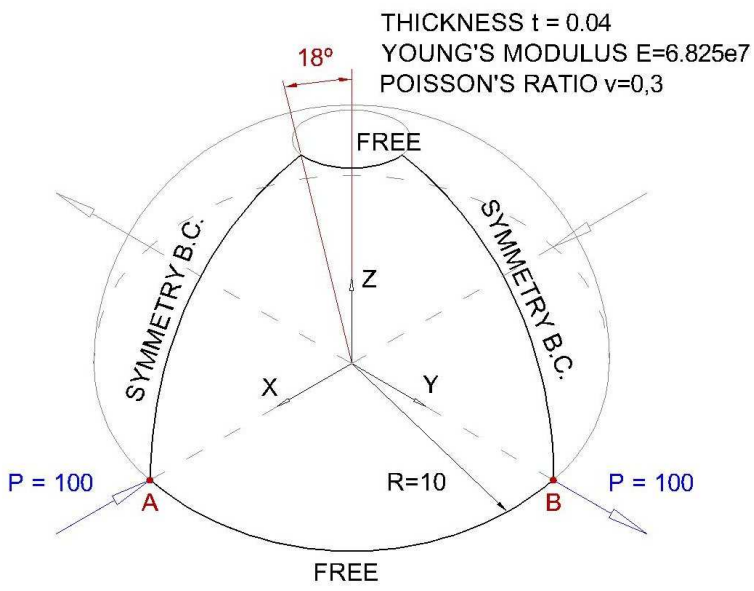

The thickness of the cylinder is lower than 1/100 of its radius, so the structure can be considered a thin shell.

The accessible reference solution does not refer to any mesh distribution, so different regular meshes were tested with the double purpose of check the convergence and compare the results with the reference result. 5x5, 10x10, 20x20 and 40x40 quadrilateral meshes were calculated and the corresponding triangular meshes obtained by splitting the previous elements through one diagonal.

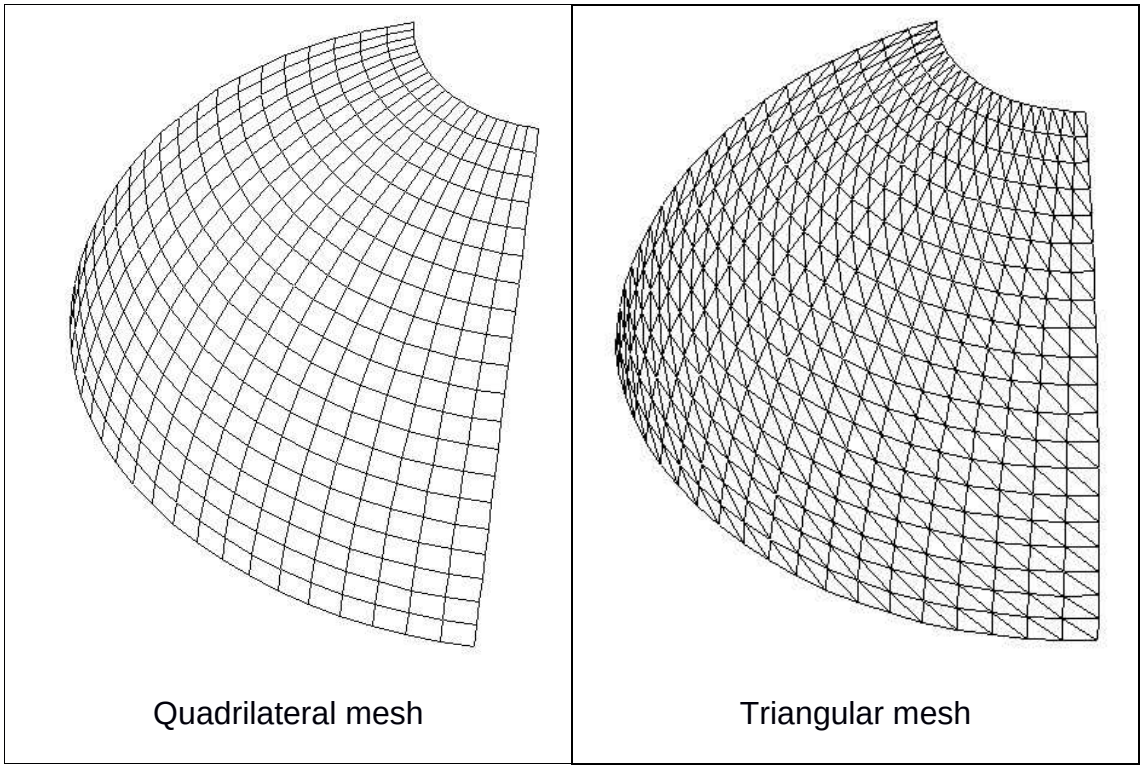


*Figure 43. Sample of the meshes used*

## Results

The following figures show the last step of the incremental deformation for a quadrilateral 20x20 mesh.

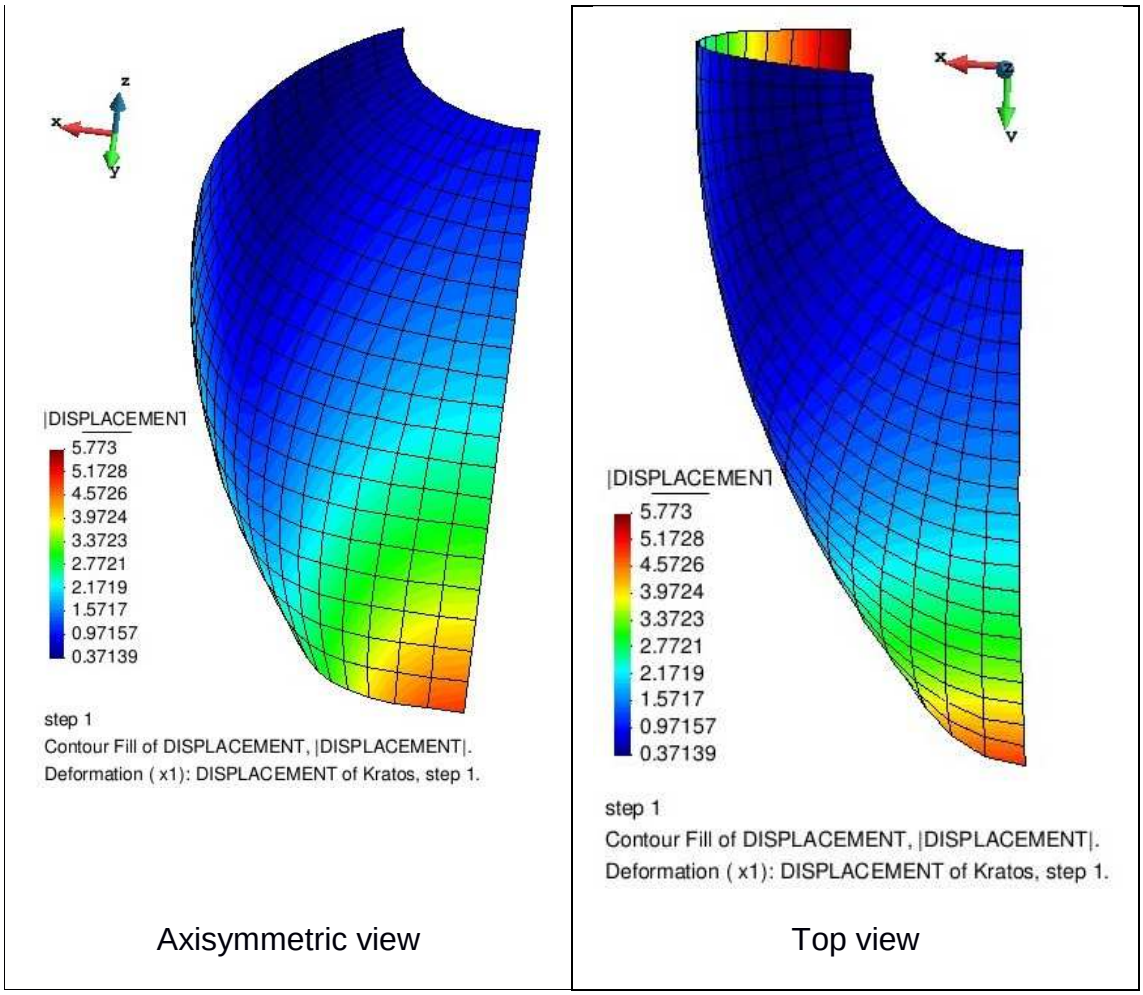


*Figure 44. Deformed final state*

A part from the final deformation step, the non-linear evolution is also of interest. The points fixed to check the evolution in time are the 2 points of the base of the hemispherical section coinciding with the x and y axis, which have opposite elongation / contraction sign.

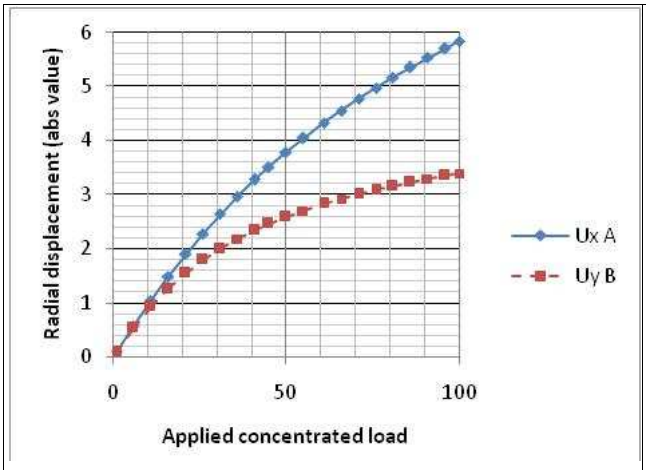


Kratos numerical solution

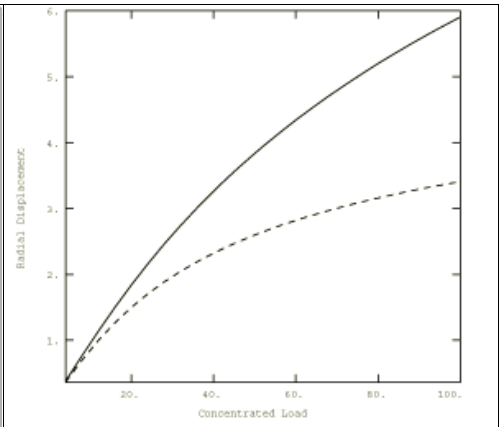

Reference numerical solution NAFEMS

*Figure 45 Radial displacement evolution Kratos and reference solution from the NAFEMS publications.*

The next tables show the results for the radial displacement considering the different elements, meshes, the reference solution and the difference respect the latter.

**RESULTS FOR QUADRILATERAL THICK ELEMENT**

| | APPLIED LOAD (40) | | | |
|---|---|---|---|---|
| | Ux (A) | Uy (B) | diff (Ux A) | diff (Ux B) |
| NAFEMS (S4 Abaqus ) | **-3.21** | **2.30** | | |
| Quadrilateral thick Kratos 5x5 | **-0.99** | **0.87** | **-69.16%** | **-62.39%** |
| Quadrilateral thick Kratos 10x10 | **-2.81** | **2.07** | **-12.45%** | **-9.98%** |
| Quadrilateral thick Kratos 20x20 | **-3.19** | **2.29** | **-0.70%** | **-0.22%** |
| Quadrilateral thick Kratos 30x30 | **-3.22** | **2.31** | **0.26%** | **0.52%** |
| | APPLIED LOAD (60) | | | |
| | Ux (A) | Uy (B) | diff (Ux A) | diff (Ux B) |
| NAFEMS (S4 Abaqus ) | **-4.34** | **2.82** | | |
| Quadrilateral thick Kratos 5x5 | **-1.45** | **1.19** | **-66.67%** | **-57.87%** |
| Quadrilateral thick Kratos 10x10 | **-3.76** | **2.53** | **-13.41%** | **-10.29%** |
| Quadrilateral thick Kratos 20x20 | **-4.24** | **2.81** | **-2.22%** | **-0.42%** |
| Quadrilateral thick Kratos 30x30 | **-4.28** | **2.81** | **-1.30%** | **-0.43%** |
| | APPLIED LOAD (100) | | | |
| | Ux (A) | Uy (B) | diff (Ux A) | diff (Ux B) |
| NAFEMS (S4 Abaqus ) | **-5.80** | **3.41** | | |
| Quadrilateral thick Kratos 5x5 | **-2.22** | **1.65** | **-61.79%** | **-51.68%** |
| Quadrilateral thick Kratos 10x10 | **-5.06** | **3.04** | **-12.75%** | **-10.80%** |
| Quadrilateral thick Kratos 20x20 | **-5.77** | **3.37** | **-0.47%** | **-1.23%** |
| Quadrilateral thick Kratos 30x30 | **-5.83** | **3.39** | **0.56%** | **-0.46%** |

**RESULTS FOR TRIANGULAR THIN ELEMENT**

| | APPLIED LOAD (40) | | | |
|---|---|---|---|---|
| | Ux (A) | Uy (B) | diff (Ux A) | diff (Ux B) |
| NAFEMS (S3R Abaqus ) | **-3.12** | **2.27** | | |
| Quadrilateral thick Kratos 5x5 | **-0.51** | **0.48** | **-83.68%** | **-78.72%** |
| Quadrilateral thick Kratos 10x10 | **-2.52** | **1.91** | **-19.17%** | **-15.73%** |
| Quadrilateral thick Kratos 20x20 | **-3.19** | **2.29** | **2.32%** | **0.71%** |
| Quadrilateral thick Kratos 30x30 | **-3.23** | **2.31** | **3.51%** | **1.83%** |
| | APPLIED LOAD (60) | | | |
| | Ux (A) | Uy (B) | diff (Ux A) | diff (Ux B) |
| NAFEMS (S3R Abaqus ) | **-4.15** | **2.76** | | |
| Quadrilateral thick Kratos 5x5 | **-0.79** | **0.73** | **-80.94%** | **-73.67%** |
| Quadrilateral thick Kratos 10x10 | **-3.59** | **2.47** | **-13.41%** | **-10.65%** |
| Quadrilateral thick Kratos 20x20 | **-4.27** | **2.79** | **2.87%** | **1.00%** |
| Quadrilateral thick Kratos 30x30 | **-4.30** | **2.81** | **3.67%** | **1.80%** |
| | APPLIED LOAD (100) | | | |
| | Ux (A) | Uy (B) | diff (Ux A) | diff (Ux B) |
| NAFEMS (S3R Abaqus ) | **-5.67** | **3.34** | | |
| Quadrilateral thick Kratos 5x5 | **-1.41** | **1.20** | **-75.19%** | **-63.95%** |
| Quadrilateral thick Kratos 10x10 | **-5.22** | **3.13** | **-7.86%** | **-6.42%** |
| Quadrilateral thick Kratos 20x20 | **-5.83** | **3.38** | **2.88%** | **1.17%** |
| Quadrilateral thick Kratos 30x30 | **-5.86** | **3.40** | **3.38%** | **1.74%** |

The first thing to notice is that for this test, the difference of performance and difference respect the reference is similar for the triangular and the quadrilateral case, which was not the case for the linear tests.

In both cases, the lesser load applied, the larger is the difference between the reference solution and the one computed with Abaqus. This means that the Kratos curve is slightly smoother than the one resulting from the reference element.

For both elements the solution gets close to the reference one in few refinements of the mesh. However, the reference solution is not analytical, and it can be not adopted as reference for a proper convergence analysis.

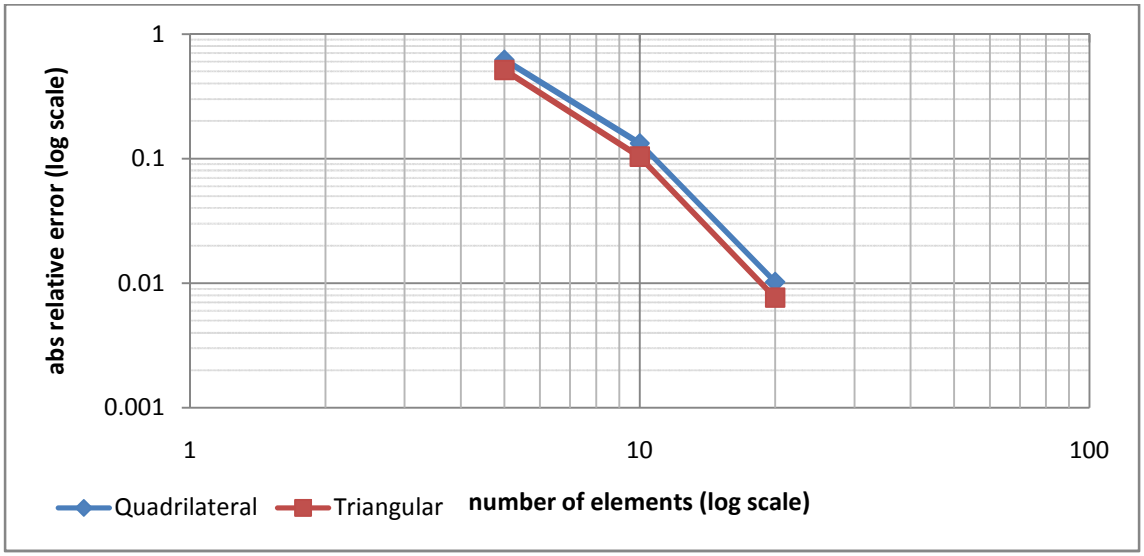


*Figure 46 convergence analysis (abs of relative error vs. n elements log scale)*

The convergence analysis was done taking the 30x30 mesh solution as the reference one in order to compute the relative error.

The slope of convergence is almost identical for both elements implemented. So taking into account all the results and comparison with the reference solution, it can be seen said that both elements performed correctly for this benchmark.

## *5.3. HINGED SPHERICAL SHEL WITH CONCENTRATED LOAD*

This test was first mentioned by G. Dhatt. 1970 [28]. It is one of the simpler benchmark in order to check the correctness of an element in a post-buckling scenario. Also, the Xfinas validation manual was used, as a source of reference results, since no analytical solution is known for the problem.

The fact of being a concentrated load, allows us to enforce a nodal displacement rather than a load, and capture the entire equilibrium path without needing any line search algorithm, which at the moment of the writing of this work was not fully integrated with the shell routines.

### Problem description

The problem consists in a curved plate simply supported on all its edges, and a punctual load is applied on the center. The curve is generated by cutting a sphere with a quadrilateral prism. The radius of the sphere is 2540mm, and the edges of the quadrilateral prism (and thus, the plan dimensions of the plate) 2*784.9mm=1569.9mm.

The thickness of the plate is 99.45mm so the thickness is over 1/10 the span of the Plate. That would lead to out of plane shear stress and transverse shear deformation cannot be neglected.

Since the problem is symmetric only 1/4 of the plate was modeled, with 2 edges simply supported B.C. and the other 2 with symmetry B.C.

*Figure 47*

*The following figure shows the geometry and material properties used for the test.*

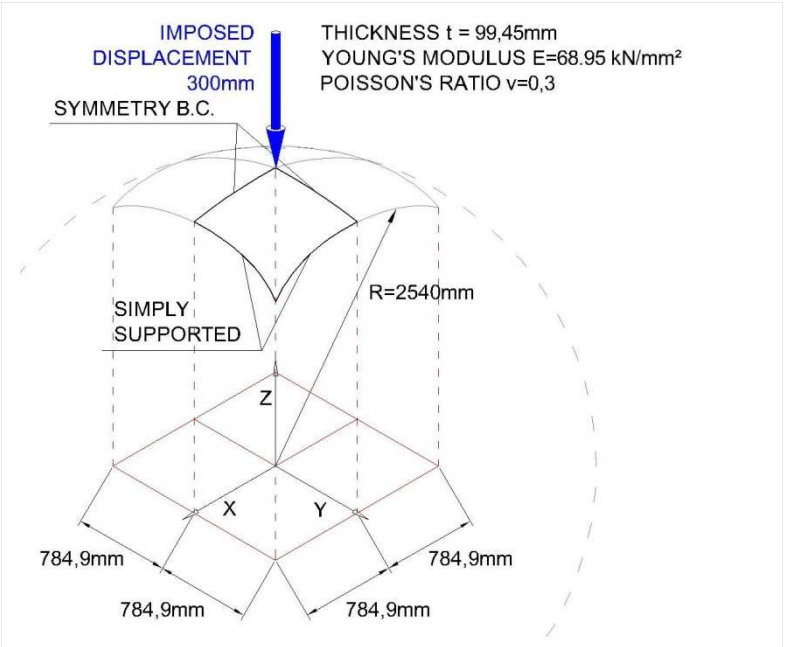


The material properties of the plate are set to young modulus 68.95kN/mm² and Poisson ratio = 0.3.

As advanced, instead of applying a nodal force in the center of the plate, an imposed displacement of 300mm was stated. This allows us to capture the same force/displacement relation without needing a line search algorithm in the post-buckling area.

The kinematic type analysis was set to Large Displacements, and a quasi-static analysis consisting in a 100 time steps incremental strategy for the imposed deformation was used in order to capture the nonlinearity of the problem.

Both quadrilateral and triangular meshes are regular ones, being 8x8 elements the reference results available for comparison. However, 4x4, 16x16 and 32x32 meshes were used to check the convergence, in both cases, and an additional 64x64 mesh in the case of the thick quadrilateral element.

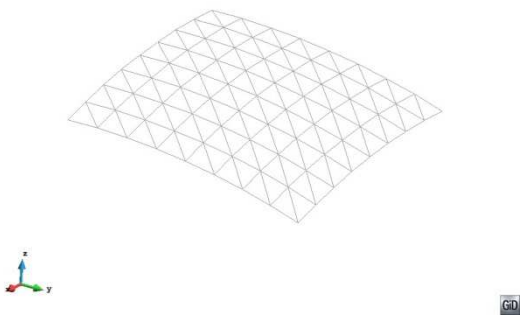

*Figure 43. Triangular mesh used*

## Results

Since we have imposed the displacement, the magnitude of interest is the shell z reaction in the center of the plate.

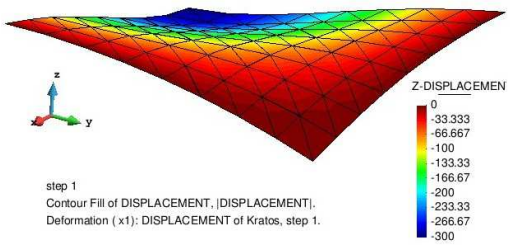


*Figure 48. Deformed final state 1x scale.*

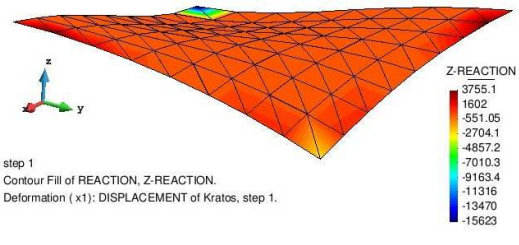


*Figure 49. Z shell reaction*

The reaction on the center of the plate for an imposed displacement is equal to the force needed in the center to generate the same displacement. We can observe in the reaction figure the concentration on the center. This value corresponds to 1/4 of the plate so adding the other 3 parts contribution is required for checking the value.

The quadrilateral thick element is using a Mindlin/Reisser formulation, and consequently we get results for the out of plane shear stress that will contribute to the deformation. On the other side, the Triangular thin element uses a Kirchhoff formulation and neglecting this effect leads to a different wrong result.

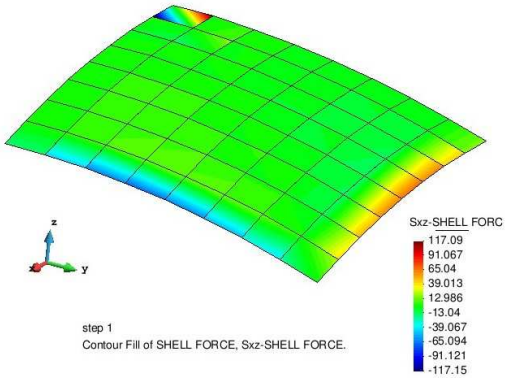


*Figure 50 Out of plane shear*

The magnitude of interest is the equilibrium path between the Load – Displacement at the center, especially the post-buckling part. The following plot shows the equilibrium path for both Kratos elements and for the Xfinas, Dhatt (1970) and Horrigmore & Bergan (1978).

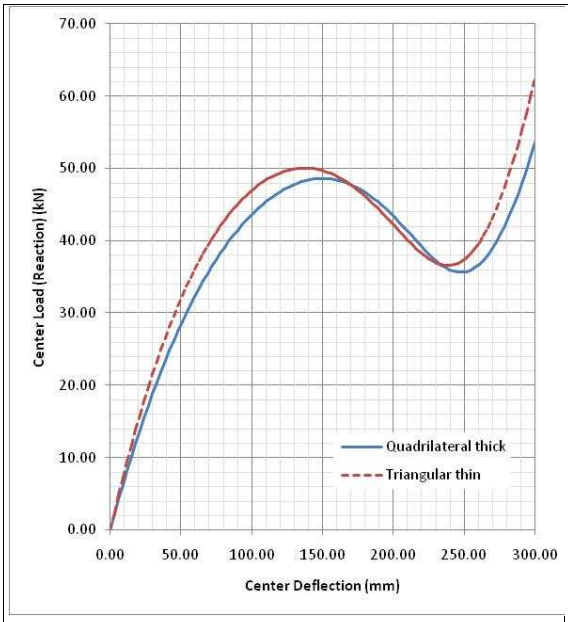


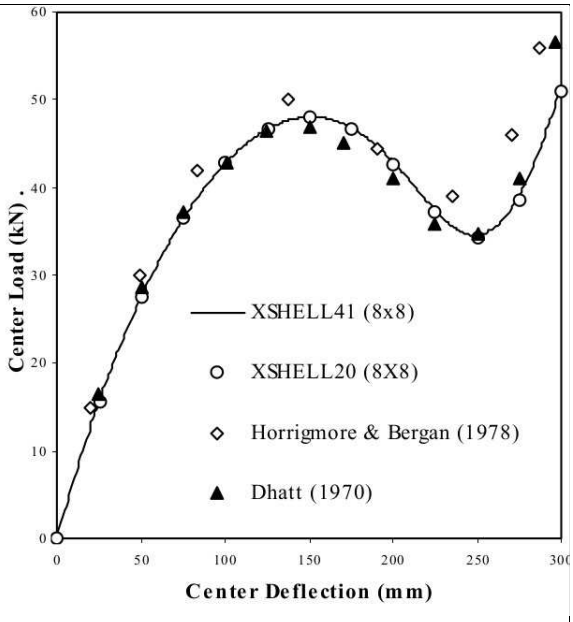


Kratos numerical solution | Reference solutions

*Figure 51 Displacement / Center Load evolution for an 8x8 mesh*

Comparison of both figures shows that the quadrilateral thick Kratos element leads to a curve that is almost identical to the one resulting for both XSHELL elements. On the contrary, the triangular thin Kratos has a significant difference and leads to a similar result than the Horringmore & Bergan (1978) one.

As a previous step to check the convergence of both elements, a comparison of the results for the different meshes was done. The following table shows the results for applied displacements of 150, 240 and 300 mm.

| RESULTS FOR Z REACTION | APPLIED DISPLACEMENT | | | LEAST SQUARES DIFFERENCE WITH PREVIOUS MESH |
|---|---|---|---|---|
| | 150.00 | 240.00 | 300.00 | |
| Quadrilateral thick Kratos 4x4 | **-50.78** | **-36.53** | **-54.90** | |
| Quadrilateral thick Kratos 8x8 | **-48.61** | **-35.97** | **-53.61** | 333.47 |
| Quadrilateral thick Kratos 16x16 | **-48.01** | **-35.69** | **-51.83** | 62.29 |
| Quadrilateral thick Kratos 32x32 | **-47.81** | **-35.72** | **-50.29** | 28.36 |
| Quadrilateral thick Kratos 64x64 | **-47.72** | **-35.88** | **-49.09** | 17.90 |
| | | | | |
| Triangular thin Kratos 4x4 | **-49.67** | **-36.23** | **-63.01** | |
| Triangular thin Kratos 8x8 | **-49.71** | **-36.59** | **-62.49** | 27.64 |
| Triangular thin Kratos 16x16 | **-49.70** | **-36.83** | **-62.52** | 2.69 |
| Triangular thin Kratos 32x32 | **-49.69** | **-36.89** | **-62.54** | 0.18 |

It is remarkable that triangular thin element converges fast; on the contrary, quadrilateral thick element keeps decreasing the values as we refine the mesh. Even though it is converging, it does so at a very slow speed.

Since the convergence is really slow, a least square comparison of the difference between each mesh and its previous one was performed, and this value is also included in the table. The least square values confirm that the convergence is on the entire equilibrium path.

The results of this convergence analysis is attached on the right

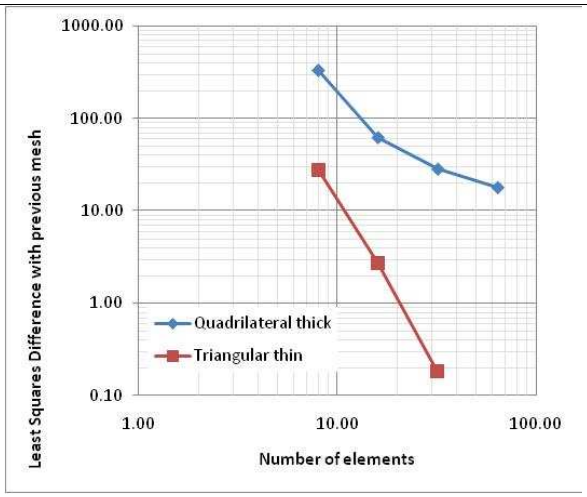


*Figure 52 Convergence analysis. (Least squares difference with previous mesh vs. n elements, log scale)*

The lack of speed of convergence could be due to the fact that the imposed displacement, resembling the punctual load, generates a reaction and transverse shear effects whose influence depends on the size of the element.

## Extension to uniform pressure

Even though the lack of line search does not allow us to make a complete full analysis, it is possible to analyze the convergence of the first limit point and a final load/displacement point after the snap through buckling for an equivalent problem subjected to uniform pressure. This analysis is performed in order to check the point that the slow convergence is caused by the dependence of the punctual loads/imposed displacements on the element size.

*Figure 53*

*The following figure shows the geometry and material properties for the equivalent problem. The plan length of the plate is 1570mm, thickness is 100mm, E=69kN/mm² and the curvature is defined by the formula*

*z=2.0285e-4·(X·(X-L)+ Y(L-Y))*

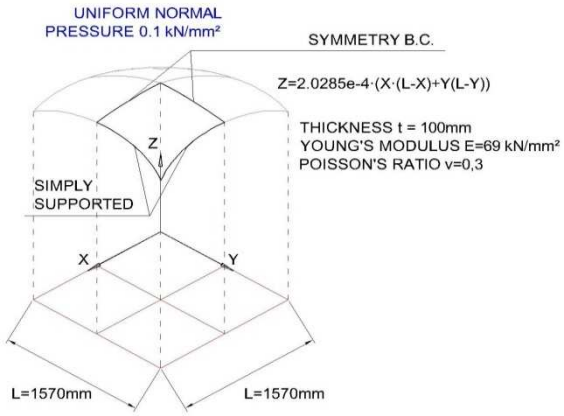


The results obtained are attached next. It must be taken into consideration that the value pre snap trough was set to the pressure step where all the meshes where stable, but with some meshes stability lasted 1 or 2 steps more, getting to deflections close to 80mm which are on the order of the results of Abaqus calculations with line search.

| RESULTS | Z DEFLECT. PRESNAP THROUGH | Z DEFLECT. FOR 0.1 PRESSURE |
|---|---|---|
| Quadrilateral thick Kratos 4x4 | **-66.32** | **308.91** |
| Quadrilateral thick Kratos 8x8 | **-68.53** | **306.12** |
| Quadrilateral thick Kratos 16x16 | **-69.77** | **305.49** |
| Quadrilateral thick Kratos 32x32 | **-70.25** | **305.36** |
| Quadrilateral thick Kratos 64x64 | **-70.39** | **305.33** |

| | | |
|---|---|---|
| Triangular thin Kratos 4x4 | **-80.25** | **303.14** |
| Triangular thin Kratos 8x8 | **-73.17** | **303.72** |
| Triangular thin Kratos 16x16 | **-71.74** | **303.83** |
| Triangular thin Kratos 32x32 | **-71.27** | **303.87** |

It is then proved that the convergence problem was due to the punctual load and not to the elements implemented.

# 6. CONCLUSION

The validation of an element is crucial in the development of any finite element software in order to ensure the correctness of the program and the accuracy of the results the final user will obtain using it. It is a process that must be made at the same time than the software itself, in order to detect and fix the possible bugs or situation where the accuracy of the mathematical model is not optimal.

The current work has focused in the validation of the elements through a first step considering linear analysis and a second one considering geometric non-linearities. Also some tools needed to make a full validation analysis are not developed for the shell case, as the line search / arch length algorithms, so the future work should be implement these tools and complete the validation process with some material non-linear .benchmarks and some more tests with line search and complex equilibrium paths.

It was found that for both element and most cases convergence for the relative error shows a 2 step curve, crossing the 0% error to get a local maximum before starting the second step with much lesser convergence slope.

The results obtained for both elements analyzed for all the benchmarks tested have been in general satisfactory compared to the reference results. It is worth to make further analysis of some of the results obtained.

For the cases of linear problems with simple stress states, both elements showed similar accuracy, and excellent performance with the only exception of the triangular element under warp distortion, which showed really poor initial results but better slope of convergence, getting similar accuracy after 2 refinements.

For the linear benchmarks with small displacements and complex stress states, the triangular thin element showed extraordinary accuracy, far better than the equivalent reference element. This is due to ANDES theory stated by C. A. Felippa. However, we have seen than even both elements obtained good results for the skew sensitivity test, the elements are more sensible to this distortion than the reference elements.

Regarding the geometric non-linearity, triangular element performed slightly better, but in the cases in which transverse shear was relevant (it has a Kirchhoff setting, so it neglects this effect by formulation). Anyway, both elements succeeded in the non-linear benchmarks; and this was the primary objective of the present work.

# 7. REFERENCES

[1] C. A. Felippa and B. Haugen C, Unified Formulation of Small-Strain Corotational Finite Elements: I. Theory, *College of engineering University of Colorado, CENTER FOR AEROSPACE STRUCTURES, CU-CAS-05-02,* 2005

[2] B. M. Fraeijs de Veubeke, The dynamics of flexible bodies, I*nt. J. Engrg. Sci.*, 14, 895-913, 1976.

[3] M. A. Crisfield, A consistent corotational formulation for nonlinear three-dimensional beam element, *Comp. Meths. Appl. Mech. Engrg.,* 81, 131–150, 1990.

[4] M. A. Crisfield and G. F. Moita, A unified co-rotational for solids, shells and beams, *Int. J. Solids Struc.,* 33, 2969–2992, 1996.

[5] M. A. Crisfield, Nonlinear Finite Element Analysis of Solids and Structures. *Vol. 2: Advanced Topics, Wiley, Chichester,* 1997.

[6] C. C. Rankin and F.A. Brogan, An element-independent corotational procedure for the treatment of large rotations, *ASME J. Pressure Vessel Technology,* 108, 165–174, 1986.

[7] C. C. Rankin, Consistent linearization of the element-independent corotational formulation for the structural analysis of general shells, NASA Contractor Report 278428, Lockheed Palo Alto Res. Lab., CA, 1988.

[8] C. C. Rankin and B. Nour-Omid, The use of projectors to improve finite element performance, Computers & Structures, 30, 257–267, 1988.

[9] C. C. Rankin, Consistent linearization of the element-independent corotational formulation for the structural analysis of general shells, NASA Contractor Report 278428, Lockheed Palo Alto Research Laboratory, Palo Alto, CA, 1988.

[10] C. C. Rankin, On choice of best possible corotational element frame, in Modeling and Simulation Based Engineering, ed. by S. N. Atluri and P. E. O'Donoghue, Tech Science Press, Palmdale, CA, 1998.

[11] C. C. Rankin, F. A. Brogan, W. A. Loden and H. Cabiness, STAGS User Manual, LMMS P032594, Version 3.0, January 1998.

[12] B. Nour-Omid and C. C. Rankin, Finite rotation analysis and consistent linearization using projectors, Comp. Meths. Appl. Mech. Engrg., 93, 353–384, 1991.

[13] B. Haugen, Buckling and stability problems for thin shell structures using high-performance finite elements, *Ph. D. Dissertation, Dept. of Aerospace Engineering Sciences, University of Colorado, Boulder, CO,* 1994.

[14] J. C. Simo and M. S. Rifai, "A Class of mixed assumed strain methods and the method of incompatible modes." *International journal for numerical methods in engineering, vol. 29, 1595 – 1638,* 2003

[15] C. A. Felippa, "A Study of Optimal Membrane Triangles with Drilling Freedoms", *College of engineering University of Colorado, CENTER FOR AEROSPACE STRUCTURES, CU-CAS-03-02,* 2003

[16] J.C. Simo, Fox, D.D. and Rifai, M.S. (1989), "On stress resultant geometrically exact shell model. Part II: The linear theory; computational aspects", *Comput. Meth. Appl. Mech. Eng*., 73, 53-92.

[17] K.J. Bathe, S. Bolourchi. Large displacement analysis of three dimensional beam structures. *International Journal for Numerical Methods in Engineering. (Impact Factor: 2.06). 12/1978; 14(7):961 - 986*. 1979

[18] L.S.D. Morley, "Skew Plates and Structures", *Macmillan Co,* 1963

[19] J. Robinson, "Basic and shape sensitivity tests for membrane and plate bending finite elements". NAFEMS C2, 1985

[20] R.H. MacNeal, R. L. Harder. A Proposed Standard Set of Problems to Test Finite Element Accuracy. *Finite Elements in Analysis Design, vol. 11, pp. 3–20*, 1985.

[21] T Belytschko, H Stolarski, W K Liu, N Carpenter, J S-J Ong, Stress projection for membrane and shear locking in shell finite elements *Computer Methods in Applied* Mechanics and Engineering 51 (1), 221-258. 1985

[22] G.Lindberg, M.Olson, G.Cowper, New developments in the finite element analysis of shells, Q.Bull. Div. Mech. Eng. Nat. Aeronaut. Establ.4. 1969

[23] A. C. Scordelis and K. S. Lo. Computer analysis of cylindrical shells. Journal of the American Concrete Institute, 61:539-561, 1964.

[24] D. G. Ashwell, R. H. Gallagher, Editors, Finite Elements for Thin Shells and Curved Members, John Wiley and Sons, London, 1976.

[25] T. J. R.Hughes, R. L. Taylor, and W. Kanoknukulchai, "A Simple and Efficient Finite Element for Plate Bending," International Journal for Numerical Methods in Engineering, vol. 11, no.10, pp. 1529–1543, 1977.

[26] T. Belytschko. “A Review of Recent Developments in Plate and Shell Elements.” Computational Mechanics—Advances and Trends, AMD vol. 75, ASME, New York, 1986.

[27] NAFEMS Publication R0024, The International Association for the Engineering Analysis Community, “A Review of Benchmark Problems for Geometric Non-linear Behavior of 3-D Beams and Shells (SUMMARY)”.

[28] G. Dhatt., An efficient triangular shell element. AIAA J., 8, 2100-2, 1970